TECHNISCHE UNIVERSITÄT WIEN
Vienna University of Technology

TRIGA CENTER Atominstitut

DIPLOMARBEIT

Tritium distribution and characteristics inside the reactor hall of the TRIGA Center Atominstitut

zur Erlangung des akademischen Grades

Diplom-Ingenieur

im Rahmen des Studiums

Physikalische Energie- und Messtechnik

eingereicht von

Martin Ibesich
Matrikelnummer 01601776

ausgeführt am TRIGA Center Atominstitut
der Fakultät für Physik der Technischen Universität Wien

Betreuung
Betreuer/in: Univ.Prof. Mag.rer.nat. Dr.techn. Georg Steinhauser
Mitwirkung: Dr. Bin Feng

Wien, 12.Oktober.2023 _____ _____

(Unterschrift Verfasser/in) (Unterschrift Betreuer/in)

Eidesstattliche Erklärung

Ich erkläre ehrenwörtlich, dass ich die vorliegende Arbeit selbstständig und ohne fremde Hilfe verfasst habe, andere als die angegebenen Quellen nicht verwendet habe und die den benutzten Quellen wörtlich oder inhaltlich entnommenen Stellen als solche kenntlich gemacht habe.

Eisenstadt, am 15.10.2023 Martin Ibesich eh

Anmerkung

Wesentliche Teile dieser Diplomarbeit wurden zur Publikation eingereicht. Die Diplomarbeit basiert auf der Publikation mit dem Namen: „Development of a Novel Passive Monitoring Technique to Showcase the 3D Distribution of Tritiated Water (HTO) Vapor in Indoor Air of a Nuclear Facility". Die eigenen Beiträge waren die Erstellung des analytischen Protokolls zur Behandlung der Proben, die Datenverarbeitung- und Auswertung aller Messungen. Das Validierungsexperiment mithilfe der aktiven Tritium - Messung ging als Projektarbeit über den Rahmen dieser Arbeit hinaus und wird deshalb auch an den entsprechenden Stellen zitiert. Aber auch hier wurde nur die Durchführung und die regelmäßige Probennahme ausgelagert. Die Datenauswertung wurde wieder eigenständig durchgeführt.

Danksagungen

Ich möchte mich hiermit herzlich bei Georg Steinhauser bedanken, der mich in seine Gruppe aufgenommen und organisatorisch sowie fachlich immer unterstützt hat. Durch seine Liebe zur Wissenschaft und seine Art Wissen zu vermitteln, werde ich immer auf eine lehrreiche, schöne und spaßige Zeit während der Erstellung dieser Arbeit zurückblicken können.

Besonderen Dank möchte ich Bin Feng zukommen lassen, der mir nicht nur die theoretischen Grundlagen gegeben, sondern auch gewissenhaft sämtliche Methoden beigebracht hat und der mir meine Fragen immer geduldig beantworten konnte. Lieber Bin, danke für die unzähligen Stunden die ich an deiner Seite lernen durfte. Ohne dich wäre das Entstehen dieser Diplomarbeit nicht möglich gewesen.

Nicht vergessen werde ich alle Mitglieder des Triga Center Atominstitutes, welche mich nicht nur sehr herzlich in ihr Team aufgenommen, sondern auch immer tatkräftig unterstützt haben und mir bei Fragen zur Seite gestanden sind.

Dabei möchte ich mich besonders bei Dieter Hainz, Monika Veit-Öller und Andreas Musilek bedanken, die mir als gute Seelen des Strahlenschutzes einige Arbeiten erleichtert haben, bei allen Problemen immer eine Lösung parat hatten und ohne die ich nie die Möglichkeit bekommen hätte diese Arbeit zu schreiben.

Ohne Frage wäre ein Absolvieren dieses Studiums ohne die Hilfe meiner Familie nicht möglich gewesen. Es gibt keine Worte, die meine Dankbarkeit ihnen gegenüber entsprechend ausdrücken könnten. Mama, Papa, ich bedanke mich für euren unendlichen Glauben in mich und euer Vertrauen, welches mir auch in schwierigen Situationen immer Halt gegeben hat.

Den letzten Satz möchte ich meiner Freundin Jessica widmen, die mir über all die Jahre des Studiums beigestanden hat und die mir immer geholfen hat den richtigen Weg zu finden, wenn meine Kraft am Ende war. Ich glaube es bedarf nicht vieler Worte, um festzuhalten was sie mir bedeutet: Alles.

Zusammenfassung

Während des Betriebes von nuklearen Einrichtungen wird durch verschiedenste Aktivierungs- und Spaltungsvorgänge Tritium (^3H, $T_{1/2}$ = 12,33 a) produziert und als Tritiumoxid (überschweres Wasser, HTO) an die Umgebung abgegeben. Da es sich bei Tritium um einen radioaktiven Betastrahler handelt, muss, im Sinne des Strahlenschutzes, eine genaue Überwachung der Konzentration in Innenräumen durchgeführt werden, um die Sicherheit der Angestellten zu gewährleisten und eventuelle Leckagen zu identifizieren. Bei den derzeitig vorhandenen Systemen ist es schwierig, gleichzeitig hohe Repräsentativität, Empfindlichkeit und räumliche Auflösung zu erreichen. In der vorliegenden Arbeit wird ein passives Überwachungssystem vorgestellt, das einen neu konzipierten passiven Probennehmer enthält und ein angepasstes analytisches Protokoll für die erste umfassende 3D-Charakterisierung der HTO-Verteilung innerhalb einer nuklearen Reaktoranlage umfasst. Die Ergebnisse zeigen, dass diese Technik eine lineare Probenahme in jeder Umgebung und die gleichzeitige Vorbereitung von hunderten Proben innerhalb eines Tages ermöglicht. Die aufgearbeiteten Proben wurden danach mittels Flüssigszintillation vermessen und das gesamte Verfahren in mehreren Schritten validiert, um die Messwerte zu untermauern.

Mithilfe der dreidimensionalen Überwachungsmatrix wurden zum ersten Mal die signifikanten räumlichen Unterschiede in den HTO-Konzentrationen (75 – 946 $\frac{mBq}{m^3}$) in der Reaktorhalle des TRIGA Center Atominstituts nachgewiesen. Im Anschluss wurde mit dem Massebilanzmodell die HTO-Freisetzungsrate (3199 ± 306 $\frac{mBq}{h}$) bestimmt, mit der theoretischen Berechnung (2947 ± 254 $\frac{mBq}{h}$) verglichen, was auf einen stabilen, leckagefreien Betrieb des Reaktors schließen lässt. Dieses neuartige Verfahren stellt somit dem Forschungsgebiet der nuklearen Forensik ein validiertes kostengünstiges Tool zu Verfügung, mit dem die Verteilung und Charakteristik von Tritium in Innenräumen dargestellt werden kann.

Abstract

During the operation of nuclear facilities, tritium (3H, T1/2 = 12,33 a) is produced by various activation and fission processes and released into the environment as tritium oxide (super-heavy water, HTO). As tritium is a radioactive beta emitter, close monitoring of indoor concentrations must be carried out to ensure the safety of staff and to identify any leaks. However, simultaneously achieving high representativeness, sensitivity, and spatial resolution is challenging with current systems. This study introduces a passive monitoring system that includes a newly designed passive sampler and a tailored analytical protocol for the first comprehensive 3D characterization of HTO distribution within a nuclear reactor facility. The results demonstrate that this technique allows linear sampling in any environment and simultaneous preparation of hundreds of samples within one day. The processed samples were subsequently measured using liquid scintillation counting, and the entire procedure was validated in multiple steps to ensure the reliability of the measurements.

Using the three-dimensional monitoring matrix, significant spatial differences in HTO concentrations (75 – 946 $\frac{mBq}{m^3}$) were observed for the first time in the reactor hall of the TRIGA Center at the Atominstitut. Furthermore, the HTO release rate (3199 ± 306 $\frac{mBq}{m^3}$) was determined using a mass balance model, compared with theoretical calculations (2947 ± 254 $\frac{mBq}{m^3}$), and indicates a stable and leak-free operation of the reactor. This novel approach provides a validated, cost-effective tool for the field of nuclear forensics, enabling the visualization of the distribution and characteristics of tritium in indoor spaces.

Table of contents

1. Introduction

Radionuclides released from nuclear facilities may have an impact on human and environmental health and are likely to trigger public concerns about the nuclear industry. Therefore, comprehensive, and reliable monitoring of environmental radionuclides is essential [1,2]. Among the well-known anthropogenic nuclides, tritium (^{3}H), a radioactive isotope of hydrogen, is noteworthy due to its long half-life of 12.33 y and its high migration capacity [3-5]. In the environment tritium is present as tritiated water (HTO) as well as HTO vapor in air [6], which leads to a high distribution in the water cycle and in the food chain [7-9]. Over the past decades, several laborious monitoring campaigns in various countries have documented the airborne HTO dynamics in the atmosphere outside of nuclear facilities [10-13]. Monitoring the HTO distribution inside of such facilities serves in the framework of supervisory monitoring to investigate the state of the reactor and assess occupational exposure [14-16]. Current indoor tritium measurement systems (e.g., ionization chambers) provide on the one hand fast information about the status of the reactor, but are on the other hand very expensive, provide only a single point measurement and have a high detection limit. Moreover, their ability to provide a spatial profile of the HTO concentration inside a nuclear facility is very limited [17-19].

Lacking precise and specific data on HTO in the air, it becomes challenging to accurately identify small leakages from nuclear installations, which in turn hinders the assessment of exposure risks. Additionally, the absence of detailed information about tritium in contaminated environments can impede the development of effective strategies for decommissioning of nuclear facilities. To address potential challenges arising from the expansion of nuclear power, encompassing both fission and fusion, there is a need for a supplementary method that can comprehensively characterize HTO vapor in nuclear facilities. Such a method would enable better preparedness for the future.

A cost-effective and convenient method for monitoring airborne HTO with high spatial resolution involves a passive ^{3}H monitoring technique that combines passive sampling with liquid scintillation counting (LSC) [20-21]. This approach has gained popularity in outdoor HTO monitoring scenarios, such as radiation monitoring near nuclear facilities and baseline investigations [22-24].

However, despite its success outdoors, the application of this technique in indoor environments facing substantial tritium contamination, such as nuclear reactor halls, is not yet a routine practice [25-26]. Surprisingly, the concept of using this technique for indoor tritium monitoring was proposed back in the 1980s [27], highlighting a mismatch between the existing frameworks of passive HTO monitoring and the demands for indoor tritium monitoring. Specifically, one significant concern is the lack of consideration given to the variations in adsorbent's sampling rate after long-term exposure. Over time, nonlinear sampling can significantly compromise the representativeness of passively collected samples, making it challenging to accurately assess the indoor tritium levels [28]. Additionally, the current samplers simple design does not only hinder their adaptability in environments with fluctuating humidity but also restricts the monitoring of HTO dynamics to a two-dimensional (2D) profile, as these samplers are deployed on a horizontal plane [29,30]. Furthermore, the sample preparation process involving the desorption method through heating is deemed time-consuming and labor-intensive and dealing with hundreds of contaminated samples, it may lead to cross-contamination issues during preparation. Although leaching ^{3}H-contaminated materials is a widely used and convenient approach in nuclear decommissioning [31,32], it has not been incorporated into passive HTO monitoring frameworks due to the absence of tailored analytical protocols and method validation. Due to these challenges, the three-dimensional (3D) spatial distribution and dynamics of HTO in large buildings, such as reactor halls, remain unclear. In this thesis, an innovative passive monitoring technique was developed, validated, and implemented for indoor HTO monitoring scenarios. The primary

objective was to address the challenges, leading to the creation of a custom-designed HTO sampler and the establishment of a leaching-based protocol for rapid analysis of passively collected HTO samples. The performance of the sampling method and the radiometric properties of the leaching process were thoroughly evaluated. The feasibility and sensitivity of the technique were confirmed through real-life testing.

Subsequently, the first-ever 3D indoor HTO monitoring matrix was successfully constructed, providing a daily resolution in a reactor hall with a volume of approximately 7100 m^3. This breakthrough allowed for precise identification of HTO hotspots and estimation of the indoor HTO release rate using a mass-balance model. Furthermore, the work included an assessment of occupational radiation exposure risks associated with ^3H under both reactor operation and shutdown scenarios.

2. Theory and basic information

2.1. Physical principles

The atomic nucleus consists of only two approximately equally heavy types of particles, which are collectively referred to as nucleons. These include the neutral neutron and the slightly lighter proton, which carries a charge of +e. The number of protons is indicated by the nuclear charge or atomic number Z. Together with the number of neutrons N, this gives the total number of nucleons as A = Z + N, which is also referred to as the mass number of the nucleus. When two atoms have the same atomic number but different numbers of neutrons and atomic masses, they are called isotopes [33]. The binding of nucleons is achieved through the strong interaction, which is many times stronger than the Coulomb force and gravitational force. In general, the total energy and mass of two attracting bodies decrease due to the Einstein relation $E = mc^2$. In connection with this, the binding energy is defined as the energy released during the synthesis of a nucleus from its nucleons. Whether a nucleus is stable or undergoes decay depends on the binding energies of the daughter nuclides and the parent nuclide, following the principle of energy conservation. If the total binding energy of the daughter nuclides is higher than that of the parent nuclide, radioactive decay occurs. This is because only in this case energy can be released [34].

Radioactive decay always occurs due to a change in an atom's nucleus by the emission of particles or electromagnetic radiation. These emissions include alpha particles (alpha decay), beta particles (beta decay) or gamma rays (gamma decay) [36].

- Alpha decay:

In alpha decay, a helium nucleus, which consists of two protons and two neutrons is emitted. This process is energetically allowed for heavy nuclei and is responsible for the absence of stable elements with $Z > 83$.

The general relationship is written in the following equation:

$$^{A}_{Z}X_{N} \rightarrow {}^{A-4}_{Z-2}Y_{N-2} + {}^{4}_{2}He^{2+} + \Delta E$$

A part of the released binding energy ΔE is available to the helium nucleus as kinetic energy after the decay. The remaining energy is emitted to the environment as gamma radiation.

In radiation protection, special attention must be paid to alpha particles due to their high biological impact [34].

- Beta decay

In beta decay, a distinction is made between beta-minus (β-) and beta-plus (β+) decay, depending on whether a nucleus has an excess of neutrons (β-) or a deficiency of neutrons (β+) to achieve balance [34].

In β- decay, an electron and an electron antineutrino are emitted:

$$^{A}_{Z}X_{N} \rightarrow {}_{Z+1}{}^{A}Y_{N-1} + e^{-} + \nu_{e}$$

In β+ decay, a positron and an electron neutrino are emitted:

$$^{A}_{Z}X_{N} \rightarrow {}_{Z-1}{}^{A}Y_{N+1} + e^{+} + \nu_{e}$$

- Gamma decay

After a radioactive decay (e.g., alpha decay), the daughter nuclide is often in an excited state. Upon transitioning from this excited state to a lower-energy state, the released energy is emitted as gamma radiation. In most cases, the nucleus remains in the excited state for only a few picoseconds, but it can also persist for a longer time, as in the case of Ba-137m, which is referred to as an isomeric transition. Gamma radiation consists of high-energy photons that move at the speed of light. Due to their high energy, shielding with dense materials such as lead or uranium is required [34].

2.2. Properties and production of tritium

Tritium (^3H) is a radioactive isotope of hydrogen and possesses one proton and two neutrons in the nucleus with a half-life of 12.33 years. It occurs in the same physicochemical form as hydrogen is ubiquitous in the environment and is a beta emitter which decays with the emission of a beta radiation with 18.6 keV maximum energy into ^3He [3,37].

Every year about 7.2 x 10^{16} Bq of tritium are naturally produced in the earth's upper atmosphere through the interaction of cosmic rays with nitrogen molecules ($^{14}_7N(^1_0n, ^3_1H)^{12}_6C$) [37,38]. By taking the half-life of tritium into account, the equilibrium inventory of naturally produced tritium in the atmosphere is approximately 1.29 x 10^{18} Bq or 3.6 kg [39].

After production, tritium is mainly present as HT but may be oxidized in the atmosphere to HTO and takes part in the global water cycle [37].

Besides the natural production in the atmosphere, several human activities in the last century raised the tritium levels in the atmosphere. Anthropogenic tritium is generated in nuclear facilities like nuclear reactors, fuel reprocessing or tritium manufacturing. Significant amount of man-made tritium, around 520-550kg were injected into the stratosphere by atmospheric nuclear weapon tests in the 1950s and 1960s [3]. Due to the ban of nuclear weapon tests in the atmosphere in 1963 (PTBT), the main sources for anthropogenic tritium in the present are nuclear reactors [37]. Here it is produced by neutron activation of some components of the reactor like the Water coolant and moderator, the Helium coolant, the Graphite moderator and the U and Pu fuel. Mainly with the following reactions [38]:

- $^2H(n,\gamma)^3H$
- $^3He(n,p)^3H$
- $^6Li(n,\alpha)^3H$
- $^{10}B(n,2\alpha)^3H$

2.3. Basics of liquid scintillation counting

The basis of the detection of radioactive substances by means of scintillation is the possibility to excite atoms. This means raising the energy level of the atom to an energetically higher state than the stable ground state. When falling back to the ground state, some atoms can emit energy as light, which is then used as a measure for the number of excitations. In case of ionizing radiation as the cause of excitation, the emission of light is a measure of the activity.

The scintillator is the material that is excited by the sample. This can be either in solid or liquid form. Solid scintillators are mainly used for the detection of gamma radiation. Liquid scintillation counting (LSC) is a preferable technique for low level activity measurements in a variety of scientific fields for alpha and beta radiation. For measurement, the radioactive sample is dissolved in a liquid solution called cocktail. This cocktail is made up of the aromatic, organic solvent on the one hand and of the scintillator material on the other hand. The alpha or beta particles emitted by the radionuclides release their energy via collisions with the molecules in the aromatic, organic solvent. This causes them to shift to a higher energy level. The energy is then transferred to the scintillator material, which also gets excited and emits light when it falls back to the ground state.

A beta particle that triggers an interaction in the scintillator leaves a trail of excited solvent molecules on its way, which generate a trail of excited scintillator molecules. Each scintillator molecule produces only one photon, and its wavelength is characteristic for the scintillator material and not for the activity of the sample. The quantity of photons produced is directly linked to the distance traveled by the β particle, which is influenced by its released energy by interaction with the solvent molecules. The strength of each light signal corresponds to the release energy, while the frequency of the signals per second corresponds to the quantity of radioactive emissions.

The emitted light pulses are then detected by a photocathode photomultiplier system, amplified and processed as a signal [36].

Especially for soft beta emitting nuclides, like tritium, LSC has several advantages compared to other applications which results in a higher counting efficiency. These include [40]:

- 4π geometry due to the fact that the sample is completely surrounded by the detection solution
- no radiation absorption by air or counter windows between the sample and the detector
- no self-absorption of radiation

2.3.1. Signal processing and analysis

The signal is first processed by the photocathode photomultiplier system and then evaluated with a pulse height analysis. Typically, a pair of photomultiplier tubes is used to capture the emitted light from the scintillation vial. This approach aims to enhance the signal-to-noise ratio of the sample counts. In most cases, when an ionizing event occurs, light photons are detected simultaneously by both photocathodes. The coincidence circuit is specifically designed to generate an output signal only if it receives input pulses from both photomultipliers within approximately 1 microsecond. Random electronic noise pulses occurring in one photomultiplier tube rarely coincide with those in the other tube, thus they are discarded. This process increases the ratio of the actual count rate to the electronic noise rate, consequently boosting sensitivity. The magnitude of the output pulse is directly proportional to the energy dissipated in the liquid scintillator. This allows for pulse height analysis and facilitates radiation spectroscopy [40].

The scintillation counter categorizes every burst of photons based on the photon count, which corresponds to the energy of the individual β particle emission event. These bursts are sorted into channels, and the counts per minute (CPM) within each channel are recorded. Each channel represents a specific range of β particle energies and counts with energies outside the predetermined limits are excluded from that channel.

Typically, three channels are selected, dividing the energy spectrum of emissions into low, medium, and high energy ranges. The lowest channel corresponds to the energy of ^{3}H emissions, the intermediate channel to ^{14}C and the highest channel corresponds to ^{32}P.

Once all the counts have been compiled, the radiation intensity, expressed as CPM, and the energy distribution or spectrum are available for use. The CPM value is proportional to the quantity of the isotope in the sample, while the spectrum gives a hint towards the identity of the isotope.

In an ideal scenario, within a cocktail solution, all the energy from a single β particle would be collected and converted into light. The emitted β energy spectrum and the disintegrations per minute (DPM) values could be directly derived from the data. The highest energy emissions could be compared to the known maximum emission energies of specific radioisotopes to confirm the identity of the isotope. However cocktail solutions are not 100% efficient in collecting and converting energy, especially with lower energy β emissions. This adds complexity to the interpretation of the data [36]. Figure 1 illustrates a block diagram of a liquid scintillation counter.

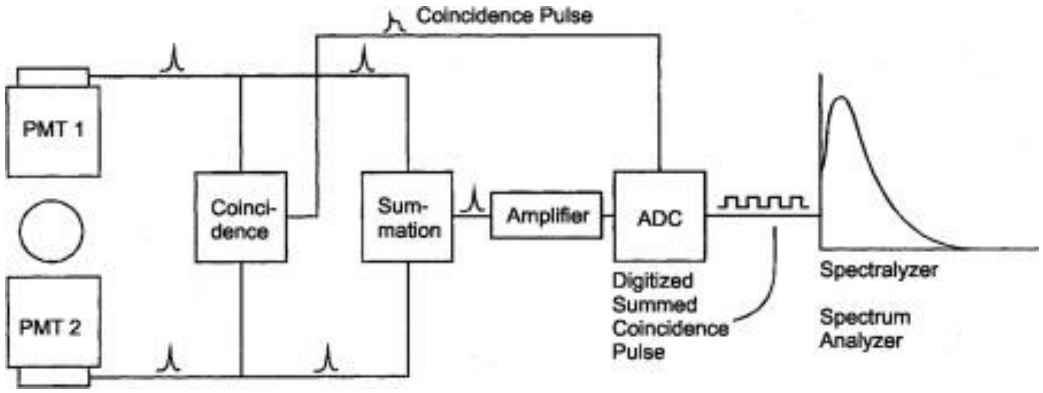

Figure 1: Block diagram of liquid scintillation counter taken from [12]

2.3.2. Counting efficiency and quenching

While there are different ways to quantify the effectiveness of a scintillation cocktail, it is commonly measured as the counting efficiency, which represents the percentage of emission events that result in a detectable pulse of photons. Counting efficiency is calculated as CPM/DPM, the ratio of Counts per Minute (CPM) to Disintegrations per Minute (DPM), expressed as a percentage. The counting efficiency varies depending on the isotope, sample composition, and the specific scintillation counter used. The poor counting efficiency can be attributed to the low conversion rate of energy to light, even under optimal conditions. It has been estimated that only approximately 4% of the energy from a β emission event is converted to light, even with highly efficient scintillation cocktails. Fortunately, this conversion efficiency remains relatively consistent across a wide range of β-energies, which simplifies signal interpretation. However, due to the low energy conversion efficiency, low energy β particles generate only a few photons. For instance, ^{3}H, with a maximum β energy of 18.6 keV and a scintillation efficiency of 4%, would produce around 240 photons. Considering the average emission energy is generally 30-40% of E_{max}, this would result in approximately 70-100 photons. However, most phototubes used in scintillation detection can only detect 1 in 4 photons. Therefore, an average ^{3}H β-emission event would generate only a 20-25 photon pulse in the counter. Consequently, emissions below average energy or those that lose photons due to sample characteristics might fall below the detection threshold of a single photon event and go unnoticed by the instrument [36]

The reduction in CPM due to the absorption of β-energy or photons by sample components is known as quenching, which is caused by certain characteristics of the sample or scintillation cocktail. Quenching can be classified into two categories, chemical quenching and color quenching. While chemical quenchers absorb the excitation energy before it can be converted into light and decrease the number of photons generated by one particle, the color quenchers absorb light within the wavelength range emitted by the scintillator. The total number of

emitted photons remain unchanged in color quenching but the number of photons that reach the photomultiplier is reduced. To correct the quenching, several different methods can be applied. The most common used one is the use of an internal standard which is a sample with a known amount of radioactivity. This standard is added to the unknown sample and increases the DPM. The ratio of the determined DPM to the measured DPM then allows a statement about the influence of the quenching and enables the calculation of the counting efficiency for the unknown sample [36,40].

2.4. The TRIGA Mark-II reactor

The TRIGA Center Atominstitut of TU Wien operates a TRIGA (Training Research Isotope Production General Atomic) Mark-II reactor which is used for research and teaching at the TU Wien. This reactor was commissioned in 1962 and has been in operation an average of 220 days a year since then. In continuous operation, the reactor delivers a total output of 250 kW_{th}, but the homogeneity of fuel and moderator also makes it possible to pulse the reactor power for a short time. An important point is the inherent safety of the reactor due to its strongly-negative temperature coefficient. This is achieved by the special mixture of the fuel (uranium-zirconium-hydride) [35].

3. Materials and Method

3.1. Design of passive sampler

In this thesis, the primary focus of developing a new passive HTO sampler was to prioritize sampling representativeness, sampling flexibility, and sampling cost, rather than emphasizing high sampling stability or extremely low levels of detectability. This consideration stems from the fact that indoor environments near nuclear facilities typically exhibit less turbulence but higher levels of tritium contamination compared to outdoor settings. Taking inspiration from the design of cylindrical samplers utilized for sampling other pollutants, a customizable HTO passive sampler was created using readily available materials, thereby ensuring the manufacturing cost of the sampler remains economical.

Figure 2 illustrates the assembly of the main sampler body, consisting of four detachable components: a hanger, a protective housing container (with dimensions Φ71mm×119mm, Semadeni AG), a mesh cylinder (Φ30mm×85mm), and a bottom lid with a sampling hole.

The suspension head is securely attached to the protective container using a mechanical screw and a specially designed connecting shell. During operation, approximately 30 g of zeolite 4Å (Disidry® Silicagel) was loaded into the mesh cylinder. The friction forces between the shell and the opening of the mesh screen allow the two components to be physically connected. To enhance the adaptability of the samplers to different environments, a customizable bottom lid with a range of single hole diameters was utilized to control the sampling rate.

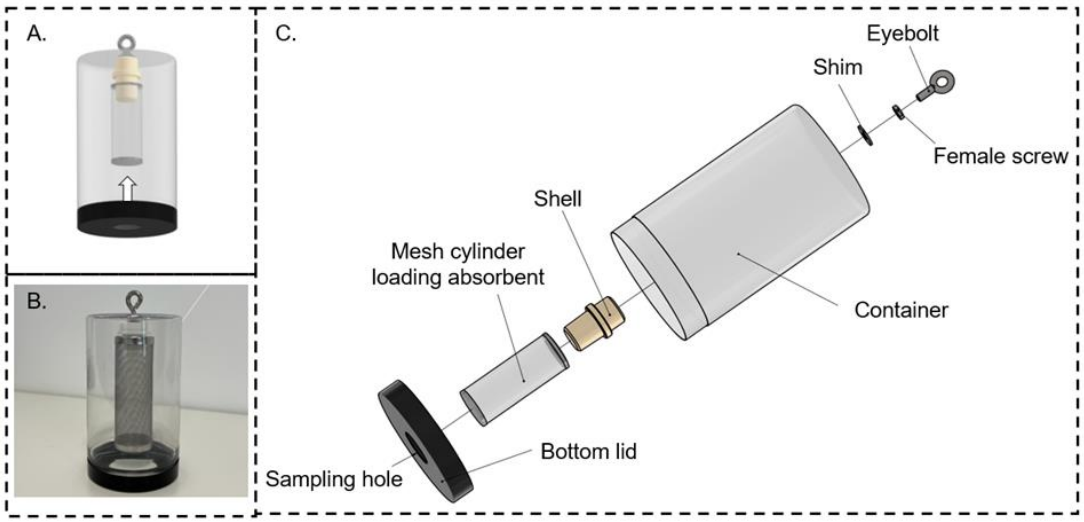

Figure 2: Sketch of the sampler design (A), photo of the sampler (B), exploded assembling drawing (C)

3.2. Analytical protocol for sample processing

For the analytical protocol in this thesis, modifications to the customized analytical protocol for leaching ^{3}H from absorbents in passive samplers, drawing from the ^{3}H analysis framework employed in nuclear decommissioning, were made [43]. The modified protocol involves three steps, which are described in detail below:

1. Leaching the utilized absorbent in a sealable baker for a specific duration. (Leaching conditions)
2. Separating the leachate from suspended particles in the leaching solution an prepare the measurement. (Measurement preparations)
3. Measure the ^{3}H activity in the leachate using commercial Liquid Scintillation Counters (LSCs). (Measurement conditions)

3.2.1. Leaching conditions

The various leaching variables have a significant effect on the properties of leachate and must be examined very closely to provide the best result. These include the leaching material, water amount, temperature and duration. The leachate recovery and the quenching level in the leachate were considered the quantitative indices of the method's operability and reproducibility. For ^{3}H analysis, approximately 10 g of sample water is required in LSC system [21], and the quenching effect should be as low as possible. All the leaching experiments were performed in a laboratory at a constant temperature (20°C).

First, the difference in the leachate properties among three common adsorbents, including zeolite 4Å (Disidry® Silicagel, 3-5 mm), silica gel without a color indicator (Supelco®, 2-5 mm), and orange silica gel with cobalt indicator (Carl Roth GmbH, 2-5 mm), were investigated. Approximately 30 g of adsorbent was placed in a sealable beaker, where a specific amount of triple distilled water was added in advance. After that, the beaker was immediately sealed, and a sealing film (PARAFILM®) was used to prevent air exchange.

To determine the specific amount of triple distilled water for leaching to collect enough leachate for measurement, the performance of zeolite leachate after adding different amounts of water was subsequently investigated. About 30 g of zeolite was added to the sealable beaker, where a given amount of triple distilled water (10, 20, 25, 27, 30, 35, 40, 45, and 50 mL) was set up. After one day, the leachate was collected, and its volume was weighted.

The influence of leaching temperature on the leachate was also investigated. The sealable beaker loaded with 30 g of zeolite and 35 mL of triple distilled water was placed in a water bath with constant temperature (50° C and 80° C) for one day and four days of leaching. The opening of the bath was covered with aluminum foil to prevent water evaporation.

Also, a two-week leaching experiment was carried out to learn how leaching duration affects the characteristics of the leachate. Approximately 30 g of zeolite was packed in a sealable

beaker with 35 mL of triple distilled water, and the leachate was then collected at 1, 2, 3, 4, 5, 7, and 14 days after the start of the experiment. In addition, a diluted tritium standard water (approximately 79.1 ± 1.2 Bq L^{-1}) was prepared to verify the recovery efficiency of tritium. About 35 mL of triple distilled water was added into a sealed beaker where about 2 mL of tritium standard water and 30 g of zeolite had reached an equilibrium. Following a similar experimental procedure, the leachate with different leaching duration was collected, and the ^{3}H levels in the leachate were determined using the LSC systems for twelve hours.

3.2.2. Measurement preparations

To prepare the samples for measurement, all residual leachate was extracted with a syringe, and the collected volume was weighted with a balance (resolution: 0.01 g). To lower the quenching effect, of suspended particles in leaching, the leachate was filtered by a syringe PDVF filter (0.22 µm, Spritzenfilter ROTILABO®). Moreover, a calibrated conductivity meter (Xylem Analytics Germany) was used to quantify the impurity levels in the leachate before and after filtration. The LSC sample was prepared using about 10 mL of filtered leachate mixed with 10 mL of scintillation cocktail (Ultima Gold LLT, PerkinElmer, USA) in a 22 mL polytetrafluorethylene (PTFE) counting vial.

3.2.3. Measurement conditions

The measurements were performed with two different calibrated LSC systems, Tri-Carb 2910RT (PerkinElmer, USA) and Hidex 300SL (Hidex, Finland). The counting window for the LSC system was optimized to achieve a low MDA and the LSC quenching curve was calibrated using the ^{3}H standard solutions (IAEA) and quenching agent (CCl_4).

Before counting, a 24-hour dark adaption was performed on all the prepared samples to reduce the potential influences caused by chemiluminescence and photoluminescence. Usually, the total counting time was divided into ten sub-counting durations with the same counting interval.

The leachates produced by triple distilled water were employed as the blank sample. Therefore, the ^{3}H activity in the investigated indoor environment (A in $\frac{Bq}{L}$) can be estimated by the equation (1):

$$A = \left(\frac{C_s - C_b}{\varepsilon \times 60 \times m_s}\right) \times \frac{(m_a + m_l)}{m_a} \times \eta \quad (1)$$

where C_s and C_b are the counting rate (cpm) of environmental sample and blank; ε represents the counting efficiency that is given by calibrated quenching curve; m_s, m_a, and m_l are the weights of LSC sample (mL), passively collected sample (mL) and leaching amount (mL). η (dimensionless) is the correction coefficient for isotopic effect, which was determined by the linearity experiment.

The combined uncertainty in ^{3}H activity (U, $k = 1$) due to the errors caused by the components in equation 1 is estimated by the error propagation equation (equation 2). For the radiation measurement, the error due to statistical fluctuations during counting time was estimated on the Poisson distribution (equation 3) [21]. With respect to the introduced error during sample weighting, the standard deviation of multiple measurements was used as the error. The 95% confidential interval of the calibrated quenching curve was adopted to estimate the error of counting efficiency at different quenching levels.

$$U = \sqrt{\sum \left(\frac{\partial A}{\partial x_i} \times u(x_i)\right)^2} \quad (2)$$

where $\partial A/\partial x_i$ and u (x_i) are the sensitive coefficients and the standard uncertainty for each error component, respectively.

$$U(C) = \sqrt{\frac{C_i}{t_i}} \quad (3)$$

where C_i and t_i are the counting rate (cpm) and counting time (min) of the prepared LSC samples (i.e., environmental samples and blank samples).

3.3. Validation of radiometric properties of leaching method

Before the tritium distribution in the reactor hall was investigated, the performance of the analytical protocol must be tested. This included the adsorption of the passive sampler to understand the uptake behavior, the linearity of the samples to make sure the measured value will not change over time and the minimum detectable activity for the measurement devices.

3.3.1. Adsorption kinetics of passive sampler

To learn the adsorption kinetics of the passive sampler, calibration experiments were conducted in an unoccupied, temperature stable office. A meteorological measuring device (ZOGLAB) was placed in proximity to the samplers to capture real-time changes in temperature and humidity. It recorded data at intervals of 2 minutes. The passive samplers were prepared in the usual manner and were fitted with different-sized bottom lids (ranging from 20 mm to 60 mm) to control the sampling rate. To ensure reliability, three identical samples were employed for each sampler design. The amount of water vapor absorbed was measured using a calibrated balance (Kern & Sohn GmbH, 0.01 g).

The adsorption kinetic curves were established by gaining weight (W in g) and accumulated humidity exposure (g m^{-3} min) [23].

$$W = W_{\text{equ}} \times (1 - e^{(-a \times \overline{AH} \times t)}) \quad (4)$$

where W_{equ} is the equilibrium amount of adsorbent (g), $\overline{AH}$ and t are the average humidity and deployment time of exposure so that their production represents the accumulated humidity exposure. a is the fitting parameter related to the total mass transfer resistance. Therefore, the average humidity during exposure can be back estimated using the calibrated adsorption curve and gaining weight of adsorbent. The volumetric HTO concentrations (mBq m^{-3}) in air can be then estimated by $A \times \overline{AH}$.

3.3.2. Linearity test of the leaching method

To test the linearity of the leaching method, a series of diluted ^{3}H standards with different activities (~80, 100, 500, 5000, and 10000 Bq L^{-1}) were prepared by combining the mother ^{3}H standard with triple distilled water. For each concentration level of ^{3}H, approximately 2 mL of the standard solution was injected into a beaker, and the added amount was accurately measured using a precise balance (Sartorius GmbH, 0.01 mg). Subsequently, around 30 g of zeolite 4Å was added to the beaker, which was then sealed for a duration of 24 hours. The established leaching procedure was employed for sample preparation and subsequent analysis of ^{3}H. The isotopic effect was quantified by determining the slope (η) of a linear regression ($Y = \eta * X$) between the ^{3}H activities in the leachate (X in Bq L^{-1}) and the added solution (Y in Bq L^{-1}). To evaluate reproducibility, three sets of samples were prepared. Furthermore, these samples were retested after one and four months from the initial preparation to assess their long-term stability.

3.3.3. Minimum detectable Activity for leaching

As mentioned above, the minimum detectable activity (MDA) is an important factor in liquid scintillation counting. The MDA of the leaching method with counting time (t in min) was estimated by equation (5):

$$MDA = \frac{(2.71+4.65\sqrt{C_b \times t})}{\varepsilon \times 60 \times m_s \times t} \times 1000 \times \frac{(m_a+m_l)}{m_a} \quad (5)$$

where C_b are the counting rate (cpm) of the blank sample; ε represents the counting efficiency (%); m_s, m_a, and m_l are the weights of the LSC sample (mL), passively collected sample (mL), and leaching amount (mL).

3.4. Evaluation of passive monitoring technique

Before the application in reactor hall, the feasibility of the developed technique was validated by an active sampling system and the technique's sensitivity was also examined in real scenarios with varying tritium contaminations.

3.4.1. Co-comparison experiments with active monitoring [45]

The feasibility of the developed technique was validated by a homemade active sampling system consisting of a well-calibrated sampling pump (AirChek TOUCH, SKC) and three-stage gas-wash bottles. A 7-day comparison experiment was conducted in the ^{3}H-contaminated environment where three passive samplers (diameter of 40mm) and the active sampling system were simultaneously deployed for collecting the airborne HTO daily. Figure 3 shows the setup of the co-comparison.

Figure 3: Active and passive monitoring instruments used in the co-comparison experiment [45]

In the active sampling system, approximately 300 mL of triple distilled water was distributed into three gas wash bottles to effectively capture atmospheric HTO vapor (with an efficiency of over 99%) [44]. A consistent flow rate of 2 L min^{-1} was maintained during all active

monitoring batches. To minimize tritium memory effects from previous sampling, the used bottles were thoroughly cleaned three times with distilled water after each monitoring campaign.

In the passive sampling system, each passive sampler was loaded with approximately 30 g of spherical zeolite 4Å (sized 3-5 mm) before use. Quality assurance and quality control measures (chapter 3.5) were also implemented during sample transportation and storage in this process.

Following the sampling phase, the total accumulated sampling volume displayed on the pump was recorded, and the residual water from the three bottles was combined in a fresh container. Approximately 10 mL of this water was transferred into a 22 mL counting vial and mixed with 10 mL of scintillation cocktail (Ultima Gold LLT). By utilizing both, the total water volume and accumulated sampling volume, the concentration of HTO in the air could be estimated. For the passively collected samples, the established protocol was employed for sample preparation and analysis. The ^{3}H activities in these prepared samples were measured using the Tri-Carb 2910RT for a duration of 7-12 hours. In each counting batch, a blank sample was included to measure the dynamic background counting rate.

3.4.2. Sensitivity validation in different environments

For the sensitivity validation, passive samplers were deployed in four different rooms (Figure 4) at the TRIGA Center Atominstitut to test the distinguishing ability of the passive monitoring technique for tritium contaminations. In accordance with radiation protection regulations, all four rooms under investigation are equipped with a 24-hour ventilation system. However, it is anticipated that there will be significant variations in the levels of tritium due to the presence of potential sources in some of the rooms.

The office (a) and the reactor control room (b) are expected to have relatively low levels of tritium since there are no tritium sources in the surrounding area. In the radiochemical laboratory (c), there is a potential risk of ^{3}H contamination as a tritium labeling experiment

was conducted in the room just one day prior to our investigation. The radioactive waste storage room (d) is considered to have relatively high levels of tritium contamination due to the presence of contaminated materials and a sealed container holding tritium sources in the room.

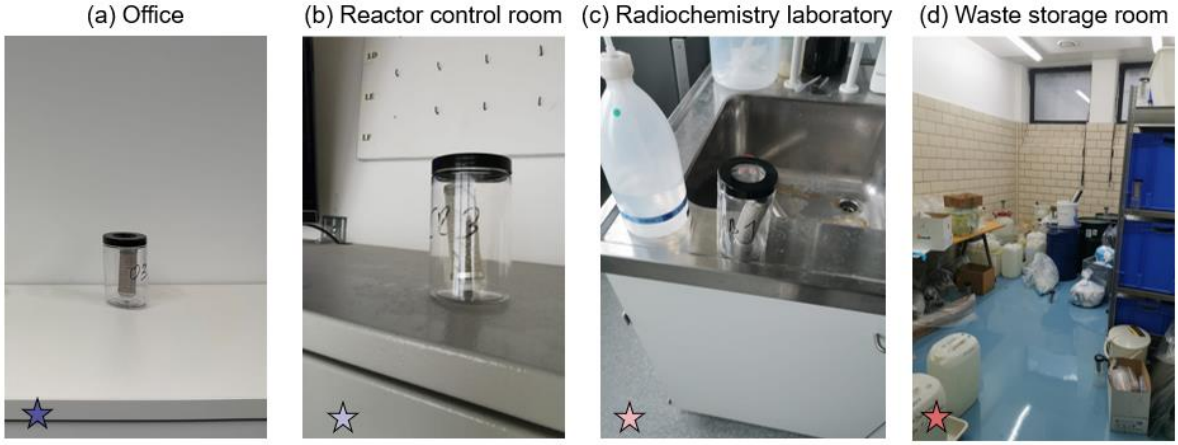

Figure 4: Exposure experiments conducted in different rooms at the TRIGA Center Atominstitut, TU Wien. (a) an office; (b) reactor control room; (c) radiochemical laboratory; (d) radioactive waste storage room

3.5. Quality assurance and quality control

Stringent quality control procedures were implemented for both laboratory studies and field investigations. The adsorbent material underwent a pre-drying process in an oven at 60 °C for 48 hours and was subsequently stored in a vacuum-sealed drying container. Prior to usage, the equilibrium state of the adsorbent was assessed to ensure that any residual water in the material would have a negligible impact on the adsorption process. In each batch of experiments, approximately 3.5 g of spherical zeolite 4Å (with a diameter of 3-5 mm) was exposed for several days in a laboratory digestor, and the uptake was measured to calculate the equilibrium load (i.e., equilibrium uptake divided by the initial weight of the adsorbent). The results indicated that the equilibrium load of the zeolite remained relatively stable as shown in Table 2.

Table 2. Equilibrium load of zeolite 4Å used in different experimental batches.

No.	Fresh weight (g)	Equilibrium weight (g)	Uptake (g)	Equilibrium load (%)[1]
1	3.56	4.32	0.76	21.35
2	3.52	4.3	0.78	22.16
3	3.49	4.26	0.77	22.06
4	3.51	4.29	0.78	22.22
5	3.52	4.29	0.77	21.88
6	3.54	4.33	0.79	22.32
7	3.54	4.33	0.79	22.32
8	3.51	4.28	0.77	21.94
9	3.52	4.29	0.77	21.88
10	3.54	4.35	0.81	22.88
Mean ± SD (k = 1)				22.1% ± 0.4%

1. Equilibrium load = Uptake/Fresh weight *100%

To prevent any potential influence from ^{3}H-contaminated water on the analysis of ^{3}H, the tritium levels in triple distilled water were evaluated before leaching the adsorbent. This was done to ensure the accuracy of the ^{3}H analysis and avoid any confounding effects. The results indicated that the blank water used in this thesis remained relatively stable and comparable (as shown in Table 3, with values of 1.96 ± 0.27 for Tri-Carb 2910RT and 13.03 ± 0.27 for Hidex 300SL). In the leaching process, a sealing film (PARAFILM®) was employed on the leaching beaker to minimize the evaporation of the leachate from the gap between the beaker and the top lid.

Table 3. Background counting rate for Tri-Carb 2910RT and Hidex 300 SL in our laboratory.

No.	LSC system	Used sample (mL)	Counting time (min)	Counting rate (cpm)
1	Tri-Carb 2910RT	10.01	840	1.91
2		10.00		2.01
3		10.02		1.93
4		10.00		1.92
5		10.00		2.07
6		10.01		1.94
Mean ± SD (k = 1)				1.96 ± 0.06
7	Hidex 300SL	10.01	840	13.19
8		10.00		13.39
9		10.02		12.69
10		10.00		13.05
11		10.00		12.90
12		10.01		12.98
Mean ± SD (k = 1)				13.03 ± 0.24

To assess the reliability of the measured results from two Liquid Scintillation Counting (LSC) systems, the same samples were cross-analyzed and compared. Furthermore, a laboratory comparison was conducted with the Österreichische Agentur für Gesundheit und Ernährungssicherheit GmbH (AGES) to evaluate the performance of the LSC systems. Both ^{3}H samples prepared by our laboratory and ^{3}H standards prepared by AGES were measured using three LSC systems: Tri-Carb 2910RT, Hidex 300SL, and Quantulus 1220. It is important to note that data points exceeding two standard deviations from the average value were excluded as per default practice in LSC analysis. The results (shown in Figure 5 and Figure 6) demonstrate that the ^{3}H specific activity provided by the two LSC systems is generally comparable, and the values measured by our LSC systems also align well with the values obtained by the Quantulus 1220 at AGES.

During field investigations, the sampler assembly was performed on-site, where the adsorbent sealed in a beaker was transferred to a mesh cylinder. This process was carried out to prevent additional water vapor adsorption during sample preparation. Similarly, immediately after sampling, the used adsorbent was promptly sealed in the beaker to minimize any additional sampling prior to sample preparation. These precautions were taken to maintain the integrity and accuracy of the collected samples in the field.

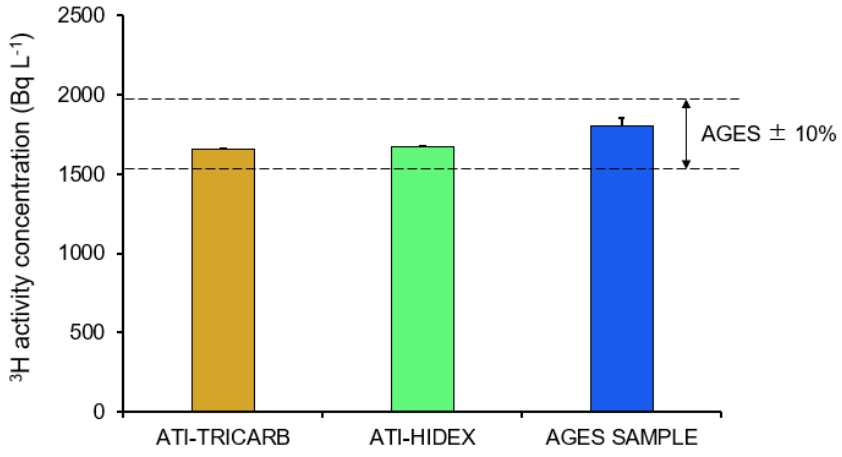

Figure 5: Cross comparison of 3H measurement in different LSC systems using AGES sample. The dosh lines are the area of ±10% error of the 3H specific activity referred to AGES

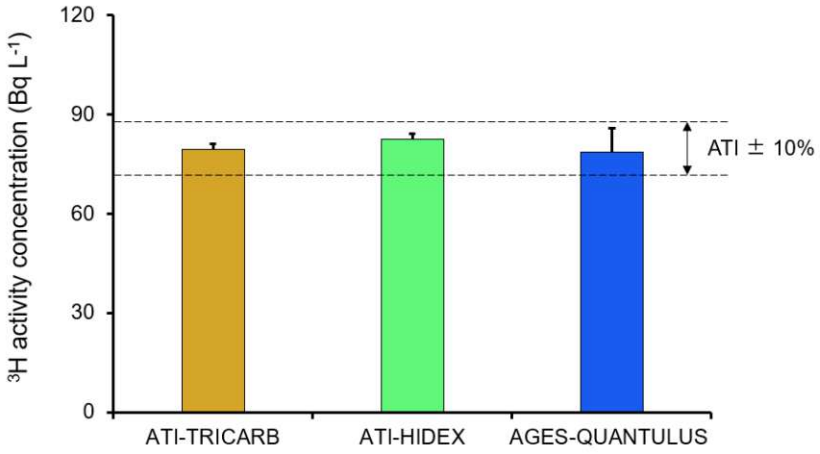

Figure 6: Cross comparison of 3H measurement in different LSC systems using ATI sample. The error bars shown in ATI and AGES represent the uncertainties of 24-h measurement (k = 2) and 7-h measurement (k = 1), respectively

3.6. Field Application

3.6.1. Reactor investigation and model calculation

To construct the 3D indoor HTO monitoring matrix in the TRIGA reactor hall, five passive samplers were fixed to a cable (~ 25 m) by latches to generate a "2D sampling matrix". Setting the position of the bottommost sampler as a horizontal reference, a constant spacing between the remaining four sampler layers was adopted to 3.5 m. Because of a slope at the roof of the reactor hall, the distance between the topmost sampler and the fixed position (lamp) was further adjusted to allow all top samplers to be at the same height. A total of 95 samplers were fixed on 19 sampling cables, which physically divided the reactor hall (~ 7100 m^3) into 95 sub-monitoring regions (Figure 7). Meanwhile, three passive samplers were deployed near the opening of reactor pool to quantify the HTO levels at the central. After one-day sampling, the ^3H contents were analyzed using the established protocol. The monitoring matrix was used during the reactor shutdown due to safety considerations.

Figure 7: 3D monitoring matrix for airborne HTO investigation in the reactor hall of TU Wien

The midpoint connection between each sampler and the adjacent sampler is considered the virtual boundary. Each sub-volume could be estimated by measuring the dimensional data with a laser rangefinder (Bosch Professional) to establish a coordinate system to describe the relative position of the samplers (Figure 8).

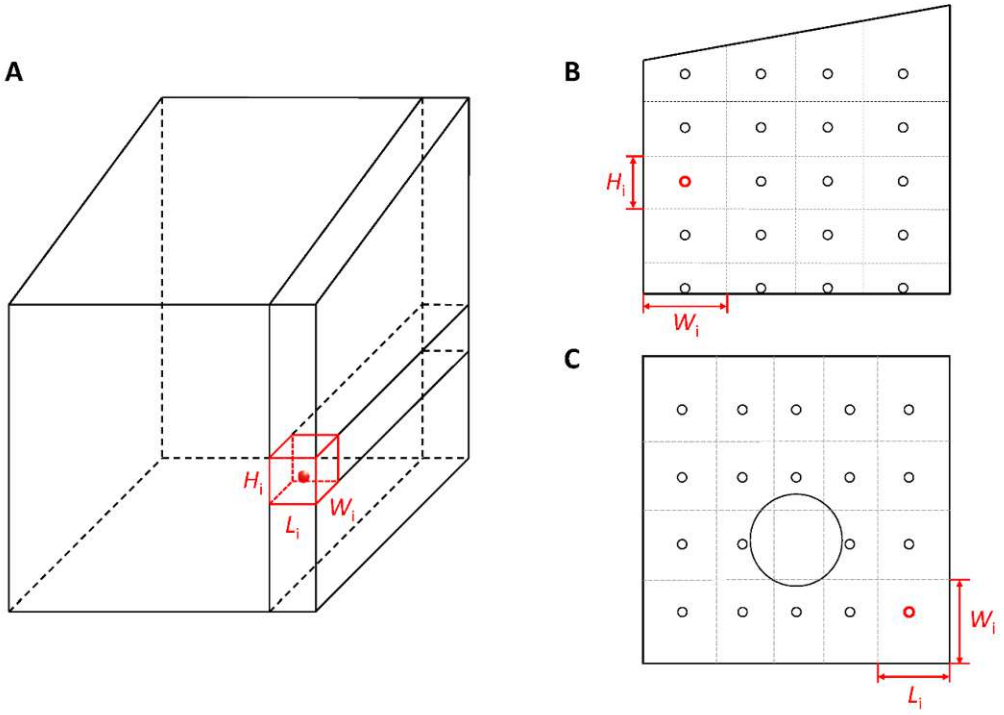

Figure 8: Explanation for the airborne HTO inventory estimation in the reactor hall. (A) Schematic diagram of a sub sampling volume. (B) and (C) are the side view and top view of the monitoring profile. The red point represents the location of a passive sampler

It should be noted that the height difference of about 2 m in the roof from the entrance to the distal end was considered in the calculation, resulting in the larger volume of those "boxes" located at the topmost layer than those in the lower layers. Limited by the spatial resolution of the monitoring matrix, the airborne HTO concentration (in mBq m^{-3}) was assumed homogeneous within each sub-volume. Therefore, the total HTO inventory in the air (I, Bq) could be estimated by Equation 6. Using Equation 7, the volume-weighted airborne HTO concentration (Cv, mBq m^{-3}) can be calculated by the HTO inventory and the total volume of the reactor hall (V, m3).

$$I = \sum_{i=1}^{95}(L_i \times W_i \times H_i \times C_i) \quad (6)$$

$$C_v = \frac{I}{V} \quad (7)$$

where L_i, W_i, and H_i are the length (m), width (m), and height (m) of a specific sub-volume box. C_i is the corresponding volumetric HTO concentration (mBq m^{-3}). The uncertainty caused by the tritium measurement was considered in the error propagation equation (Equation 2) for the total uncertainty estimation in the HTO inventory and volume weighted HTO concentration (k =1).

Combining the recorded ventilation rates and investigated HTO data, the indoor HTO release rate in the reactor hall was calculated using the one-compartment mass balance model which has been widely used for estimating the pollutant flux in the indoor environment. In this scenario, because there is no tritium generation during the shutdown stage and dominant tritium input was contributed by the evaporation, we consider the tritium emission was at steady state. Therefore, according to the description by Alodie Blondel and Hervé Plaisance [46], the volume-weighted airborne HTO concentration for the steady-state case can be obtained from the following equation:

$$C_{\mathrm{v}} = \frac{aP}{a+k} C_{\mathrm{o}} + \frac{Q_{\mathrm{HTO}}}{V} \times \frac{1}{a+k} \quad (8)$$

where a is the air exchange rate by the ventilation system (h^{-1}), and k is the net rate of the removal process by physical decay of tritium (h^{-1}). P is the fraction of outdoor ^3H penetrating the room (100%), and Co is the ^3H concentration in the outdoor environment (~ 6 mBq m^{-3}). Q_{HTO} is the total HTO release rate in the reactor hall (Bq h^{-1}).

Considering that the ventilation rate in the reactor hall (2.77 h^{-1}) is about five orders of magnitude higher than the ^3H removal process by physical decay (6.42×10^{-6} h^{-1}), equation 8 was then simplified. Therefore, the total HTO release rate can be calculated by equation 9, and the total uncertainty of Q (k = 1) was estimated using the error propagation equation with the error from the available components.

$$Q = (C_{\mathrm{V}} - PC_{\mathrm{o}}) \times V \times a \quad (9)$$

To verify whether there is a significant tritium leak from the nuclear reactor, the tritium release rate was estimated by the theoretical evaporation model, in which the HTO evaporation by the reactor pool is hypothesized to be the dominant ^{3}H input in the reactor hall. Because the tritium has similar physicochemical properties as hydrogen, the assumption that the evaporation of HTO is like the water vapor evaporation was made. In this case, by using the American Society of Heating and Air-Conditioning Engineers (ASHRAE) handbook method (equation 10) [47], the evaporation rate of water vapor ($Q_{water\ vapor}$, kg h^{-1}) from the opening pool with a diameter of 2 m can be obtained.

$$Q_{\text{water vapor}} = 0.000144 \times \left(P_{\text{pool}} - P_{\text{air}}\right) \times \left(\frac{2}{2} \times \pi\right) \quad (10)$$

where 0.000144 is the recommended coefficient in the low air velocity range (0.05 – 0.15 m s-1); P_{pool} is the saturated pressure of water vapor (in Pa) in the reactor pool; The P_{air} is the partial pressure of water vapor in the air near the reactor pool (in Pa); (2/2*π) is the opening area (in m^2) of the pool. With the concurrently recorded environmental parameters (e.g., temperature and relative humidity) inside/near the reactor pool, the Magnus-Tetens approximation (equation 11) [48] was performed here to estimate the saturated pressure of water vapor (Ps, Pa) under a specific temperature (T, °C).

$$P_s = 0.61078 \times e^{\left(\frac{17.27 \times T}{(T + 237.3)}\right)} \times 1000 \quad (11)$$

With the measured ^{3}H specific activity in the reactor pool (A_p, Bq L^{-1}) during our investigation, the theoretical HTO release rate by the water evaporation ($Q_{HTO\text{-}t}$, Bq h^{-1}) can be estimated following by Marang et al. (equation 12) [49]. The specific activity of ^{3}H in the reactor pool is considered spatially homogenous because of the operation of the internal circulation pump. Table 4 summarizes the parameters and their uncertainty used in the model calculation, and the error propagation equation was used in the total uncertainty estimation (k =1).

$$Q_{\text{HTO-t}} = Q_{\text{water vapor}} \times A_p \quad (12)$$

Table 4. The parameters and uncertainty used in theoretically estimating ^{3}H evaporation rate.

No.	Parameter	Parameter value	Uncertainty
1	Pool water temperature	29 ℃	1 ℃
2	Air temperature near the pool	23 ℃	1 ℃
3	Air relative humidity	31 %	1 %
4	^{3}H specific activity in the reactor pool	2078 Bq L^{-1}	20 Bq L^{-1}

3.7. Exposure Risk estimation

In the reactor hall, the ground floor is designated as a workspace for the physics group, occasionally also used by employees from the reactor group. To assess the internal exposure resulting from the release of ^{3}H from the reactor to these occupational workers, a survey focused on the ground area was conducted during both operation and shutdown periods to monitor the dynamics of airborne HTO. During the survey, 20 passive samplers containing approximately 30 g of zeolite 4Å were deployed at the same locations as the lowest layer of the reactor's 3D survey. After one day of sampling, the passively collected samples were analyzed using the established analytical protocol. The volumetric concentration of HTO (C, Bq m^{-3}) for each point was estimated based on the measured specific activity of ^{3}H and the humidity values calculated in reverse.

Considering that radiation regulations prohibit eating or drinking inside the reactor hall, we only consider the internal dose exposure resulting from the inhalation and skin absorption of HTO for the employees. In a hypothetical scenario, the accumulated dose from HTO (D, Sv) for an adult employee is calculated based on eight hours of work per day in the reactor hall for one year. It is important to note that this scenario represents a very conservative consideration from a radiation protection perspective and that the actual dose exposure would likely be lower than our estimation. The ^{3}H intake dose for the employee can be estimated using Equation 13 [50].

$$D = W \times DCF \times C \times R \times t \quad (13)$$

where W is the weighting coefficient considering the inhalation and skin adsorption for HTO vapor, and the value of 1.5 was adopted; DCF is the dose conversation factor for HTO, and the value of 1.8×10^{-11} Sv Bq^{-1} recommended by the International Commission on Radiological Protection (ICRP) was used; R represents the breathing rate for an adult, and the value recommended by IAEA of 3.3×10^{-4} m^3 s^{-1} was considered here; t is the exposure time in the unit of s.

4. Results

4.1. Uptake kinetics of passive sampler

During the calibration experiments, notable differences in the adsorption kinetics were observed among the samplers when adjusting the opening areas on their bottom lids. Samplers with larger openings achieved equilibrium much faster compared to those with smaller openings (see Figure 9A). By considering 35% of the adsorbent's equilibrium load as the endpoint for linear absorption, we found that the sampler with a Ø20 mm opening required approximately 18 times more accumulated exposure to reach this threshold compared to the sampler with a Ø60 mm opening. These results are consistent with previous studies [20,51] and can be theoretically explained by the lower total mass transfer resistances in samplers with larger openings, which promote the diffusion of ambient water vapor into the sampler.

Further analysis reveals that linear sampling within the humidity range of 1.85 – 33.08 g m^{-3} can be achieved using samplers with opening diameters ranging from 20 – 60 mm for one-day sampling, effectively covering typical indoor humidity scenarios [10]. This means that modifying the opening size allows for both high sampling representativeness and temporal resolution simultaneously. To facilitate better sampler opening modification in specific environments, the relationship (see Figure 9B) between the opening area (mm^2) and the maximum average humidity under one-day linear sampling (g m^{-3}), was quantitatively established. This relationship provides a valuable tool for quickly estimating the appropriate opening size based on the indoor humidity. In the experiments, a sampler loaded with approximately 30 g of adsorbent typically yielded a maximum of about 2.3 g of water sample at the linear stage's endpoint. However, the actual uptake of the sampler with a predicted opening may sometimes exceed the linear threshold due to the uneven distribution of humidity in the room. Therefore, a fluctuation within 20% of the linear endpoint still reasonable, resulting in an approximate value of ~2.8 g, was considered.

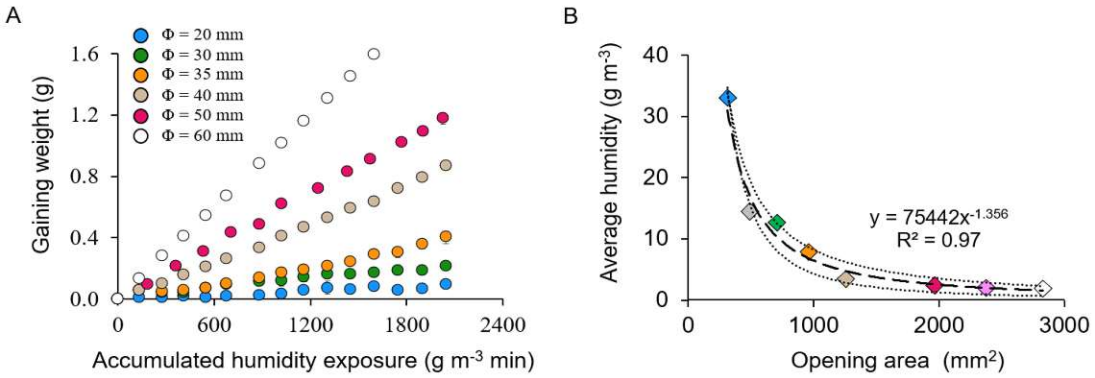

Figure 9: Uptake kinetics of passive samplers. (A) The adsorption kinetic curves of samplers with different opening areas. (B) The relationship between the opening area (mm^2) and average humidity for one-day exposure ($g\ m^{-3}$). The dot-dash lines are the 95% confidence intervals of the fitting curve.

4.2. Influence of leaching conditions on leachate

Significant impacts of leaching variables on leachate properties were observed during the batch experiments. As the ^3H analysis typically necessitates around 10 g of water samples in the LSC system [20], the leachate recovery and its quenching level were considered quantitative indices for assessing the method's operability and reproducibility. Comparing the states of zeolite and silica gel in the leachate (refer to Figure 10), the silica gel lacking a color indicator displayed a pronounced swelling effect upon water addition (Figure 10A). Conversely, the use of orange silica gel resulted in a purple-colored leachate (Figure 10B), likely due to the presence of cobalt indicator in the silica gel. While previous studies [43,52] demonstrated the feasibility of analyzing ^3H contents in leachate from trace amounts of orange silica gel (approximately 1 g), this material may not be the most suitable choice in this case. The relatively high amount of silica gel with limited leaching volume could lead to undesirable color quenching effects.

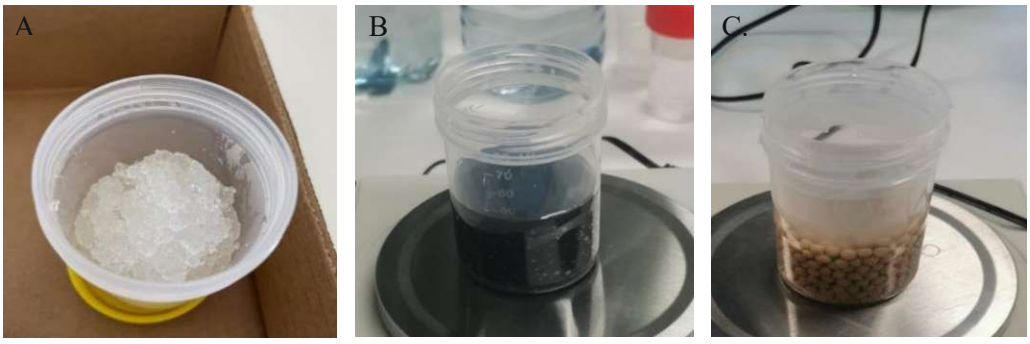

Figure 10: Silicagel without color indicator (A), Silicagel with color indicator (B), Zeolite (C)

Because of this finding, it was determined that only zeolite is suitable for field investigations, and all subsequent experiments were conducted using this material. The leaching process revealed that the visibility of the leachate is affected by the leaching material, leading to a higher degree of quenching. To address this, the leachate undergoes filtration, resulting in a clearer sample and minimizing color quenching (refer to Figure 11).

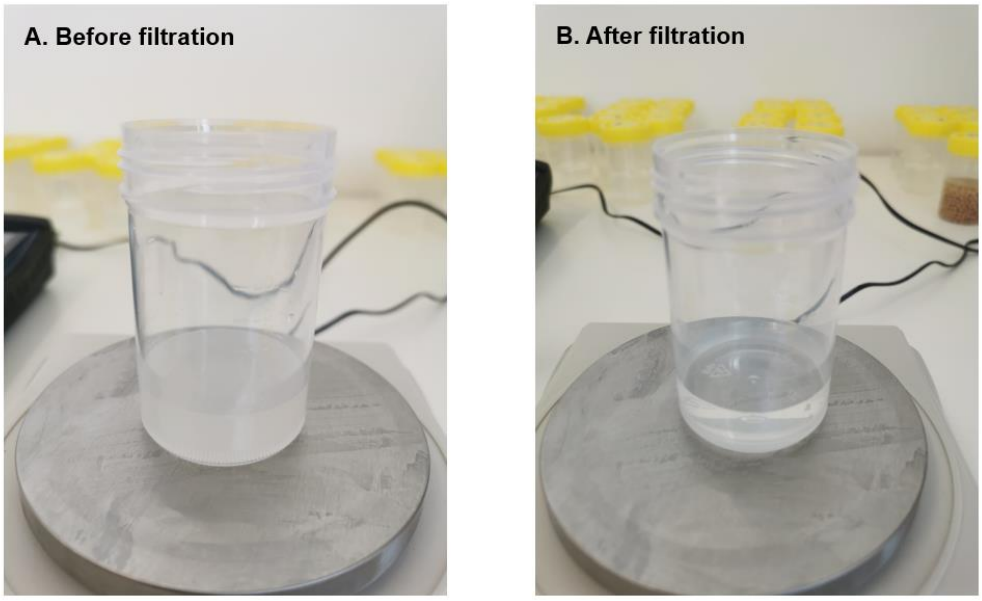

Figure 11: The visibility of leachate before (A) and after (B) using filter.

To ensure an adequate amount of leachate for ^{3}H analysis, the leaching water volume needs to exceed 25 mL (refer to Table 5). By utilizing conductivity and quenching index measurements, the physical properties of zeolite leachate were quantified under various leaching conditions. Overall, the conductivity of filtered leachate demonstrates a slight decline across all groups with different leaching volumes (see Figure 12A). Moreover, there is a significant decreasing trend in conductivity with an increase in leaching volume ($R^2 = 0.98$). Further analysis of the groups with leaching volumes exceeding 25 mL reveals a clear negative correlation between conductivity and the quenching index (see Figure 12B). This suggests that higher conductivity results in a more pronounced quenching effect in the leachate. This phenomenon can be attributed to the presence of dissolved zeolite material in the leachate, which reduces the efficiency of transporting photons in the scintillation cocktail.

Additionally, the higher leaching volume leads to dilution of turbidity, weakening the chemical quenching effect. Specific values for the conductivity can be found in Table 5.

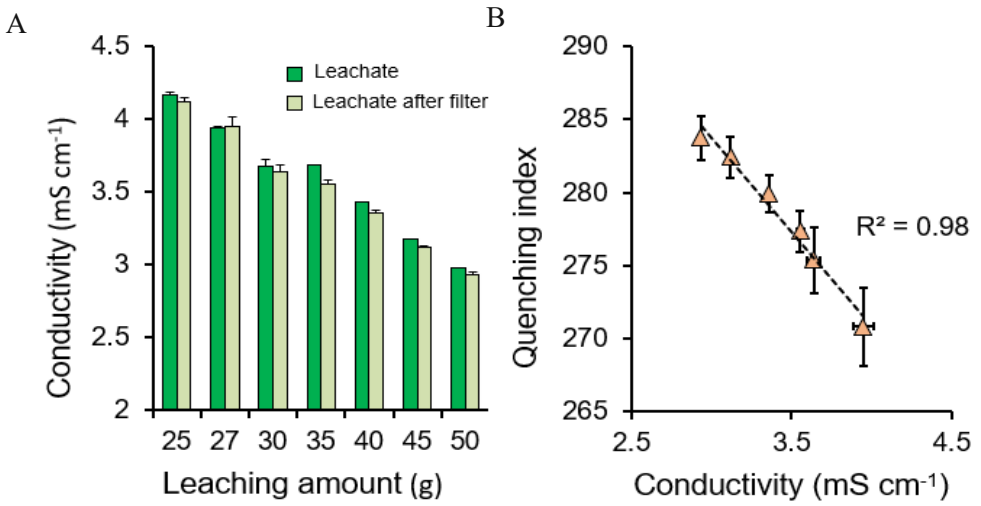

Figure 12: (A) Variation in conductivity of leachate from zeolite with different leaching amounts. (B) Regression relationship (dotted line) between the conductivity and quenching index given by Tri-Carb 2910RT

Table 5. Extracted water and conductivity in different leaching amounts.[1]

Added water (mL)	Extracted water (mL)	Filtered water (mL)	Conductivity (mS/cm)	Filtered conductivity (mS/cm)
10	0.05 ± 0.04	/	/	/
20	4.06 ± 0.09	3.59 ± 0.02	/	/
25	8.35 ± 0.08	7.98 ± 0.06	4.16 ± 0.02	4.11 ± 0.02
27	11.02 ± 0.01	10.63 ± 0.11	3.93 ± 0.01	3.95 ± 0.04
30	14.24 ± 0.19	13.15 ± 0.13	3.68 ± 0.03	3.64 ± 0.03
35	19.68 ± 0.13	19.10 ± 0.07	3.68 ± 0.02	3.55 ± 0.02
40	25.01 ± 0.07	24.68 ± 0.07	3.43 ± 0.02	3.36 ± 0.02
45	30.18 ± 0.14	26.69 ± 0.12	3.18 ± 0.01	3.12 ± 0.01
50	35.15 ± 0.08	34.70 ± 0.05	2.98 ± 0.01	2.93 ± 0.01

1. Results are presented as mean ± SD (k =1). Three replicates samples were used.

However, it is crucial to highlight that a higher leaching volume does not necessarily translate to improved analytical performance, as it could lead to a higher scaling factor, ultimately resulting in a higher Minimum Detectable Activity (MDA) (refer to Figure 13A). Considering the stability and detectability of the leachate, a leaching volume of 35 mL of distilled water proves to be more suitable in this specific case.

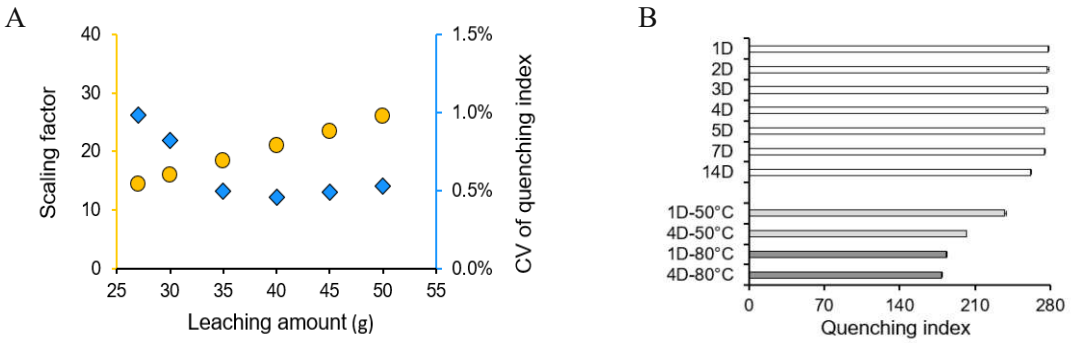

Figure 13:(A) The influence of adding leaching amount on the scaling factor (the uptake of adsorbent was set as 2 g) and the coefficient of variation (CV) of the quenching index. (B) The quenching index of zeolite and colored silica gel in different leaching durations and temperatures.

Besides the leaching amount, the duration and temperature of leaching were also observed to influence the quenching level (refer to Figure 13B). As the leaching duration was extended, the quenching index exhibited a slight declining trend ($r = -0.99$, $P < 0.01$), with the quenching value decreasing by approximately 5.3% in the case of 14-day leaching compared to 1-day leaching. Moreover, under a four-day leaching condition, the mean quenching indices were approximately 276, 202, and 178 at room temperature, 50°C, and 80°C, respectively, indicating a more significant effect of leaching temperature on quenching. These findings support the hypothesis that longer leaching duration and higher temperature promote the diffusion of solid molecules, leading to zeolite dissolution.

Consequently, for this thesis, a leaching experiment at room temperature for one day was adopted, and the final flow chart of the optimized leaching method is illustrated in Figure 14.

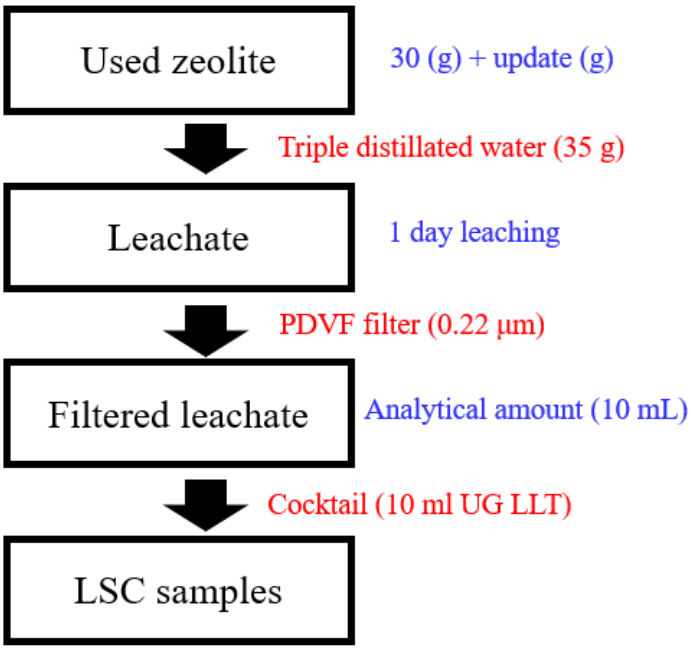

Figure 14: Flow chart of the optimized leaching method.

4.3. Radiometric properties of leaching method

As depicted in Figure 15A, the ^{3}H activity concentration in the leachates exhibited a strong agreement with the spiked ^{3}H levels (R^2 = 0.99, P < 0.01) after one-day leaching, but the slope of the fitting line (Y = 0.97 × X) was slightly below 1. Subsequent remeasurements taken one and four months after sample preparation showed minimal changes in the slope of this curve, with a coefficient of variation (CV) of approximately 2.7% (refer to Figure 16), indicating the long-term stability of the prepared samples. Furthermore, there was no significant increasing trend in the measured tritium content with increasing leaching duration (refer to Figure 15B). These results are consistent with previous findings, where about 97.84% of tritium was recovered after 24 hours in the leachate of silica gel. However, it is worth noting that the previous study used a higher 3H spike (~2×105 Bq L^{-1}) and a higher leaching ratio (H_2O: adsorbent = 3:1) [43].

Taken together, the results demonstrate that the ^{3}H recovery is independent of the original tritium contents and leaching duration. Nevertheless, to enhance measurement accuracy, a correction coefficient of 0.97 was still adopted for all measured data.

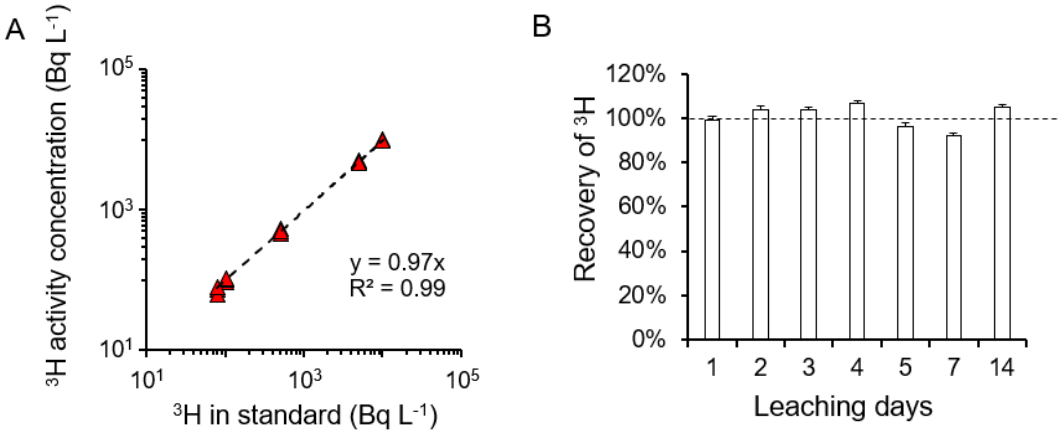

Figure 15: (A) Linearity of method, (B) Recovery of ^{3}H under different leaching days, the dotted line is the recovery of 100%, and the error bar indicates the combined uncertainty (k = 1).

.

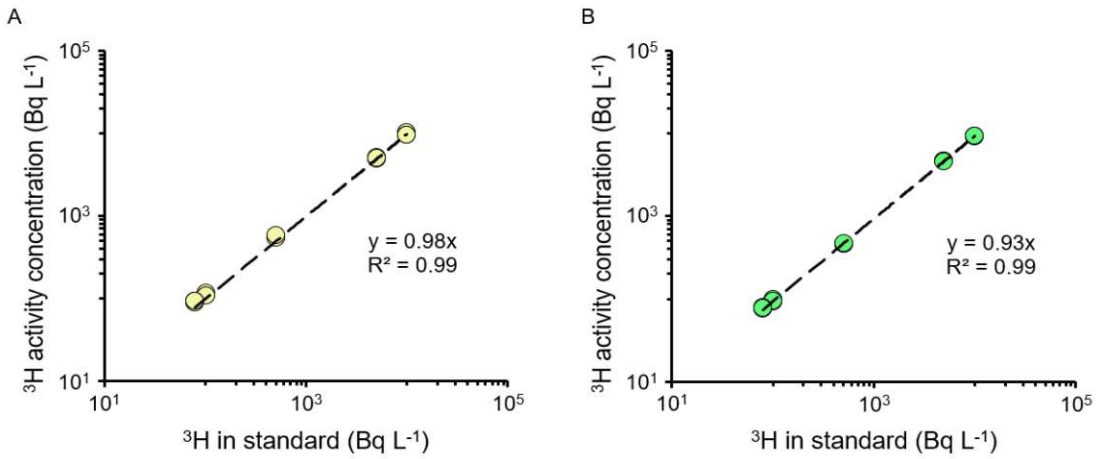

Figure 16: The linear relationship between the ^{3}H specific activity in the leachate and the spiked 3H of the standard after one month (a) and four months (b) of preparation. Each concentration point includes three replicate samples.

The MDA for the LSC system was assessed by varying the counting time and the adsorbent's weight gain. Considering that the collected water vapor typically ranges from 1.5 to 2.5 g after one-day exposure, and assuming counting durations between 6 to 24 hours, the MDA for Hidex 300 SL (refer to Figure 17A) and Tri-Carb 2910RT (refer to Figure 17B) can be estimated to be approximately 30 – 95 Bq L^{-1} and 20 – 70 Bq L^{-1}, respectively. It is worth noting that the airborne ^{3}H content in nuclear facilities varies significantly based on the monitoring location, nuclear reactor type, and operational status. However, a relatively conservative threshold of 100 Bq L^{-1} is commonly adopted as a "positive" event [53]. In this context, under a hypothetical condition with a weight gain of about 1.5 g and a ^{3}H content of about 100 Bq L^{-1}, the relative uncertainty (k = 1) would be approximately 8% and 15% after one day of counting in Tri-Carb 2910RT and Hidex 300SL, respectively. Hence, the established leaching method is deemed sensitive enough to identify ^{3}H contaminations in indoor environments. For cases with limited weight gain (e.g., 0.7 g), a longer counting duration (more than 48 hours) would be preferable to achieve the desired measurement uncertainty. In summary, the leaching method presented in this study enables rapid sample preparation and accurate determination of ^{3}H hotspots, which is expected to enhance the efficiency of tritium monitoring at contaminated sites.

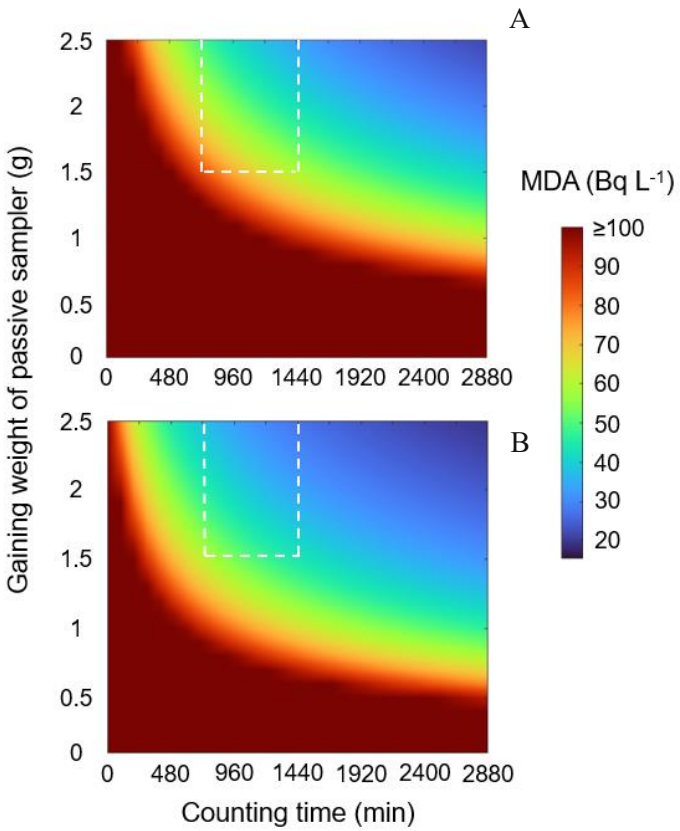

Figure 17: (A) and (B) are the method's MDA in Hidex 300SL and Tri-Carb 2910RT, respectively. The white dotted box is the MDA in the ideal region where gaining weight falls in 1.5 to 2.5 g, and the counting time is about 6–24 h.

4.4. Technique evaluation

Affected by the source term and exposure environment (e.g., flow field, temperature, humidity), airborne HTO levels often exhibit significant variations over time, underscoring the importance of carefully assessing the method's sensitivity to rapid tritium dynamics. Figure 18A presents a comparison of airborne ^{3}H concentrations determined by active and passive sampling over a ten-day period. Overall, the average air concentrations obtained from the two methods align well, with the relative standard deviation (RSD, in absolute value) generally within 20% (see Figure 18B, ranging from 1.59% to 19.72%, median: 7.1%). Within each batch of the experiment, a relatively consistent ^{3}H concentration was observed among three replicate samples, with a narrow coefficient of variation (CV) range (ranging from 7.7% to 15.3%, median: 11%). However, due to spatial differences in humidity, there was relatively greater variation in the weight gain (ranging from 0.7% to 21.3%, median: 6.8%).

These results demonstrate the feasibility of the passive monitoring technique in independently characterizing ^{3}H dynamics in contaminated environments. Further statistical analysis reveals a significantly negative correlation ($r = -0.72$, $P < 0.01$) between the CV of passive ^{3}H data and the RSD in the corresponding monitoring group. This finding suggests a limitation of the passive monitoring technique, wherein tritium contents might be slightly underestimated in scenarios with high tritium spatial variability due to its low sampling rate.

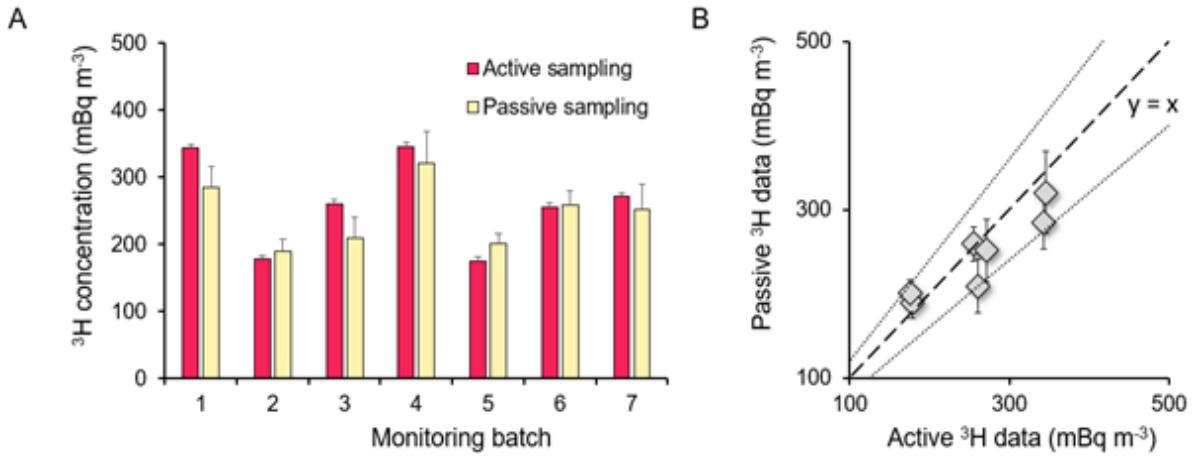

*Figure 18: (A) General comparison of ^{3}H concentration in air derived by passive and active sampling simultaneously. The error bars in active and passive groups represent the extended uncertainty (k = 2) and standard deviation (n = 3), respectively. (*B) Linear relationship between the 3H data given by passive sampling and active sampling. Two round-dot lines indicate the boundary of ± 20% uncertainty, and the long dash is the 1:1 line based on active sampling

The exposure experiments conducted in various environments demonstrate the method's high sensitivity in distinguishing different levels of ^{3}H contaminations in spatial distribution (refer to Figure 19). Monitoring results indicate that, despite a 24-hour counting period, the ^{3}H levels in the office and reactor control room remain below the detection limits. These findings align with expectations, as the continuous ventilation systems in these areas effectively dilute tritium contamination levels.

In contrast, slight ^{3}H contaminations (75 ± 22 Bq L^{-1}) were detected in the radiochemistry lab, where approximately 10 GBq of tritium material was used for a labeling experiment. Although this level of contamination falls well below the control criteria for radioactive contamination or conservative safety thresholds, the results are still valuable in demonstrating the passive method's exceptional sensitivity in screening areas with limited contamination.

Moreover, when employing a rapid screening condition with 3-hour counting, relatively high ^{3}H contents were easily identified in the radioactive waste storage room (2930 ± 1209 Bq L^{-1}) with an uncertainty below 10%. Collectively, these results confirm the significant potential of the passive monitoring technique to sensitively reflect the spatial and temporal variation/difference in ^{3}H levels in contaminated indoor environments. This capability not only aids in locating tritium hotspots and characterizing their dynamics but also provides

essential technical support for establishing a high-resolution ^{3}H monitoring matrix to assess the operational status of nuclear facilities.

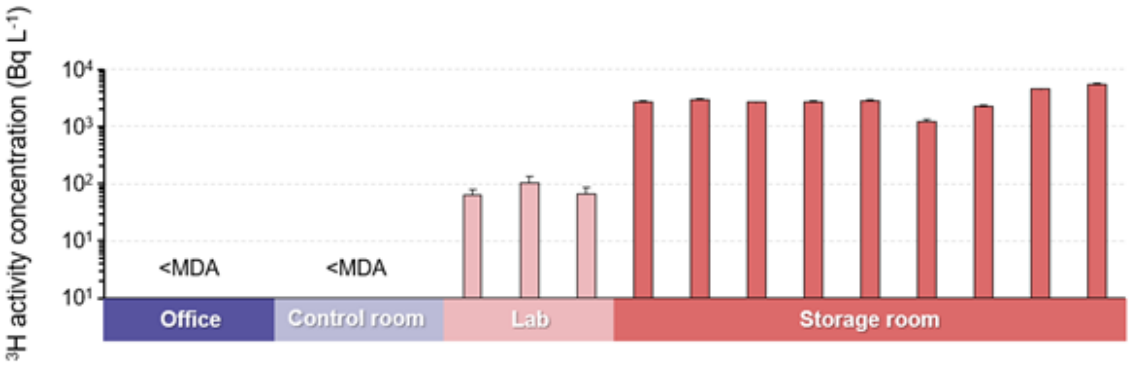

Figure 19: Results of sensitivity validation experiment conducted in indoor environments with varied ^{3}H contamination levels. The error bar is the combined uncertainty (k = 1) of passive monitoring.

4.5. Airborne HTO dynamics in reactor hall

Utilizing the first 3D monitoring matrix (refer to Figure 7), the dynamics of airborne HTO at a daily resolution were quantified (see Table A1 in the Appendix). The collected water vapor in 97 out of 98 deployed samplers fell within the range of 2.8 g (0.7 – 3.2 g, median: 1.3 g), highlighting the success of the strategy in adjusting the sampler openings according to ambient humidity, thereby enhancing sampling representativeness.

Approximately 33% of the prepared samples (32 out of 98) exhibited detectable tritium levels, showing a relatively wide variation in HTO specific activity (ranging from < MDA to 619 Bq L^{-1}, refer to Figure 20).

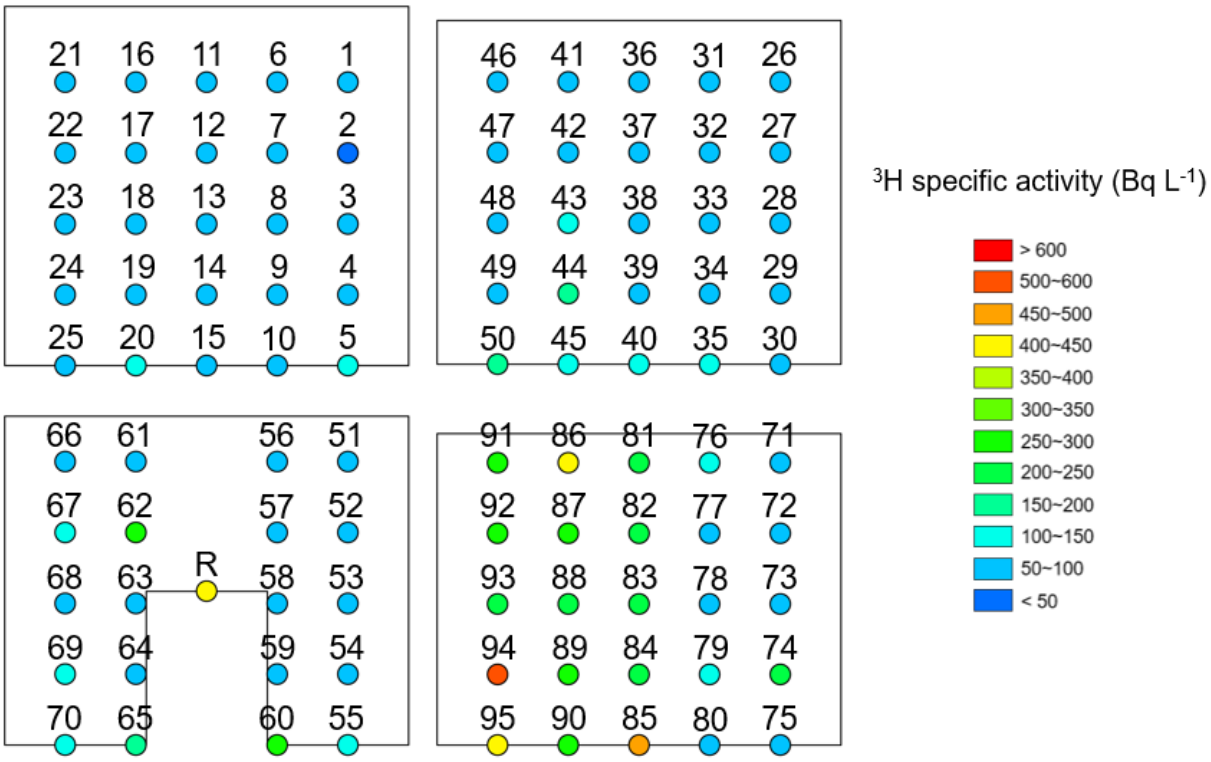

Figure 20: Spatial distribution of HTO specific activity in different vertical profiles. The value used in the reactor (i.e., R) is weighted average by the humidity of three samples.

The wide variation is not surprising since HTO can still evaporate into the reactor hall during shutdown, while the 24-hour ventilation system significantly dilutes ^{3}H contents in certain areas. However, it is important to note that airborne HTO contents vary considerably based on reactor type and operational status, as evident from previous studies reporting significant

variability in HTO levels near or within nuclear facilities in different countries. For example, studies in South Korea reported levels ranging from 24 to 1513 Bq L^{-1} [54], in France from 34 to 231 Bq L^{-1} [55], in Denmark from 20,000 to 40,000 Bq L^{-1} [43], and in Japan from 300 to 27,000 Bq L^{-1} [55]. Therefore, the measured ^{3}H contents still fall within the normal range of ^{3}H fluctuations observed in similar environments.

To better understand the tritium spatial distribution in the reactor hall, the HTO specific activity and uncertainty was set at the undetectable points to half of the corresponding MDA value [10].

The HTO volumetric concentrations for all data points were estimated using the back-calculated humidity (refer to Figure 21A). The spatial distribution profiles of ^{3}H were then visualized from the front view (refer to Figure 21B) and top view (refer to Figure 21D).

Similarly, the HTO volumetric concentrations displayed a significant variation, ranging from 75 to 946 mBq m^{-3} (median: 83 mBq m^{-3}). This value is slightly lower than the observed concentrations in the experimental reactor hall at Kyoto University, Japan (ranging from 840 to 3700 mBq m^{-3}) [57], but still higher than the general HTO baseline (around 10 mBq m^{-3}) [55]. In the vertical direction, a clear decreasing trend can be observed ($P < 0.01$) in HTO concentrations along the vertical profile from the entrance (points 71 – 95, 373 ± 187 mBq m^{-3}) to the distal side (points 1 – 25, 86 ± 11 mBq m^{-3}), indicating ^{3}H accumulation near the entrance. Additionally, in this hotspot profile, the average ^{3}H concentration on the left side (points 81 – 95, 547 ± 189 mBq m^{-3}) was significantly higher ($P < 0.01$) than the value measured on the right side (points 71 – 80, 133 ± 93 mBq m^{-3}).

Of particular interest, in the uppermost horizontal monitoring profile, located approximately 8 meters above the reactor pool port, the observed decreasing trend in HTO concentration from the entrance to the inside and from left to right persists. Notably, relatively higher tritium concentrations were recorded at points 81 (502 ± 54 mBq m^{-3}), 86 (945 ± 55 mBq m^{-3}), and 91 (478 ± 54 mBq m^{-3}), which are even slightly higher than one point near the reactor pool

port (R3, 468 ± 49 mBq m^{-3}). A possible explanation for this inhomogeneous spatial distribution is the different flow rates of the ventilation system, resulting in varied air exchange rates and, consequently, varying tritium removal efficiency at different positions within the reactor hall.

Preliminary investigations into the ventilation system seem to support this hypothesis, as the ventilation rates near the entrance are nearly one order of magnitude higher than those on the distal side, and the flow rates on the left side generally appear stronger than on the right side. Additionally, the height profile near the entrance is approximately 2 meters lower than the distal one, reducing the dilution effect by the air column, which may further increase the potential for regional tritium hotspots. While cautioning against overemphasizing the conclusion, our work suggests the possibility of secondary contamination hotspots arising from flow field differences in nuclear facilities. Further efforts, including field investigations and modeling, are necessary to study the transport process of HTO evaporated from the reactor pool within the hall.

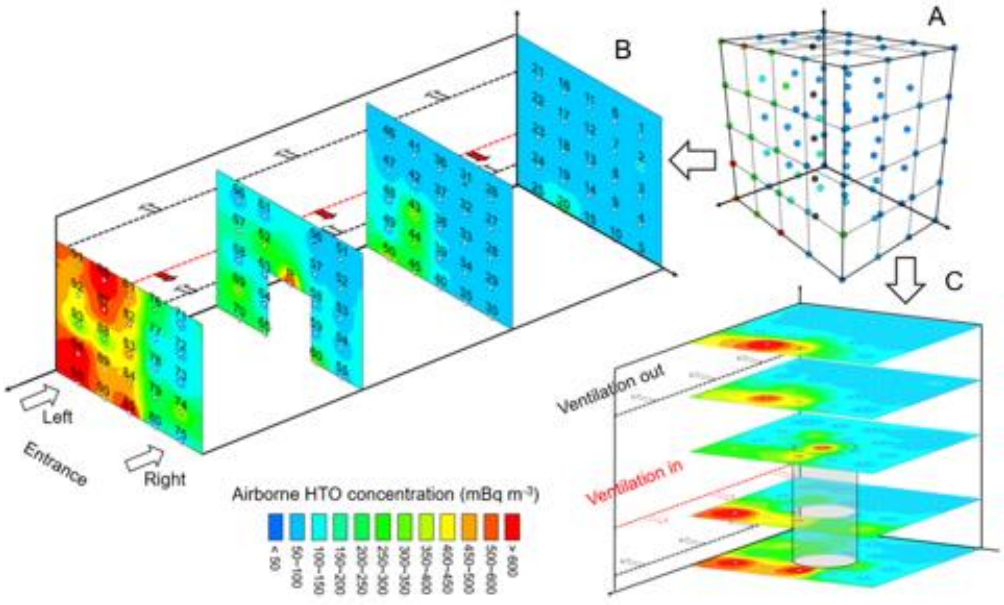

Figure 21: Spatial distribution of airborne HTO concentration in the reactor hall. (A) 3D monitoring matrix for high-resolution HTO investigation. (B) Airborne HTO concentrations at monitoring locations. (C) and (D) represent the front and top views of HTO distributions using spatial interpolation. The dosh lines are the ventilation system.

4.6. HTO release rate and exposure risk

The estimated airborne HTO inventory in the reactor hall was approximately 1.23 ± 0.06 MBq, with an average volumetric HTO concentration of approximately 172 ± 9 mBq m^{-3}. Given that the investigation was conducted one week after the reactor shutdown, employing the mass balance model, we estimated the total ^{3}H release rate from the reactor hall in the steady-state case to be approximately 3199 ± 306 Bq h^{-1}.

To evaluate the presence of any additional tritium release in the reactor hall, we further estimated the HTO evaporation rate from the reactor pool port, which is believed to be the dominant contributor during reactor shutdown. The investigation revealed that the HTO specific activity in the pool water was about 2078 ± 20 Bq L^{-1}, and using the simultaneous temperature and humidity monitoring data, we obtained a tritium input of about 2947 ± 254 Bq h^{-1} through pool evaporation. The relative deviation between the theoretical and measured values of the total ^{3}H source intensity in the reactor hall was approximately 10%, possibly attributed to an overestimation or ^{3}H concentration in the measured data, as the undetectable data was set to half of the MDA. Nonetheless, the results indicate the dominant contribution of tritium input through pool evaporation and demonstrate the robust status of the TRIGA II reactor at TU Wien.

The investigation conducted in the groundwork area shows no significant difference (P = 0.21) in HTO concentration (Figure 23) during reactor operation (254 ± 99 mBq m^{-3}) and shutdown (228 ± 156 mBq m^{-3}), further supporting the above inferences. Tritium is well-known to be produced by neutron activation in the primary coolant (i.e., pool water) of the TRIGA II reactor, and the anthropogenic tritium mainly exists in the form of tritium gas (i.e., HT or T_2) initially, rather than tritiated water. Previous work observed many bubbles in the surface pool during reactor operation [58]. The similar tritium levels at both stages could thus be attributed to the rapid removal of newly produced tritium gas by the ventilation system before oxidation occurs.

From the perspective of radiation protection, the internal exposure risks from ^{3}H at both stages (Figure 22) are limited, as the maximum dose contribution (1.4 μSv y^{-1}) remains about four orders of magnitude lower than the limits (20 mSv y^{-1}). Nevertheless, it is interesting to note that HTO levels tend to be relatively higher at the southwest corner (i.e., left entrance) during both operation and shutdown, suggesting that the flow field plays a more critical role in HTO distribution than tritium input. Therefore, deploying online tritium monitoring instruments at tritium hotspot areas, rather than random locations, would improve the efficiency of nuclear safety monitoring. Additionally, it is important to take more care of these tritium hotspots during future nuclear decommissioning, as the materials in these areas may experience more severe radiation exposure.

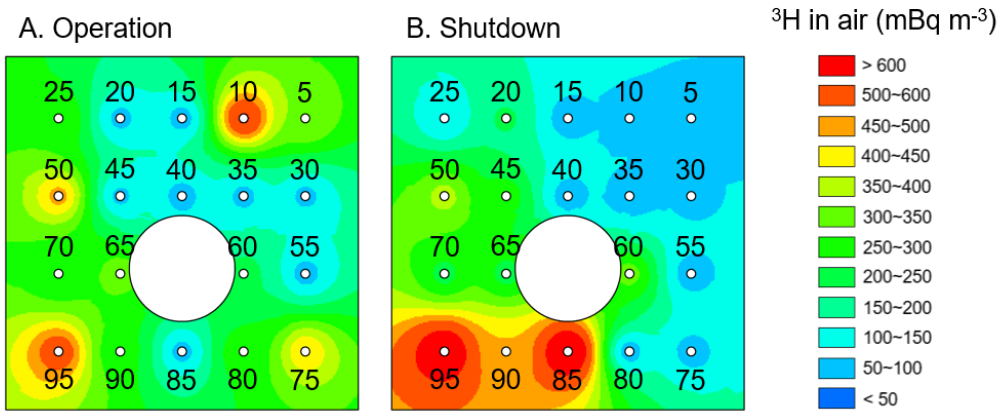

Figure 23: Spatial distribution of airborne HTO concentration in the groundwork area at operation (A) and shutdown (B) stages.

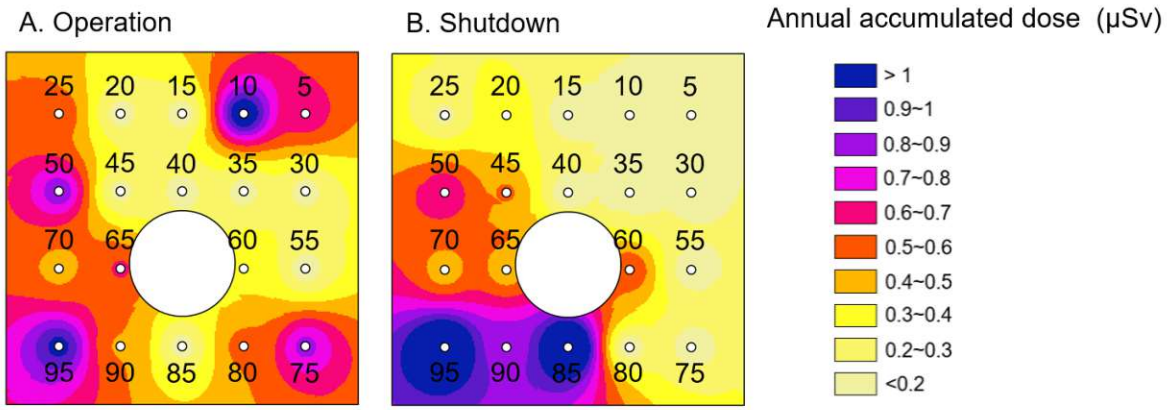

Figure 22: Spatial distribution of annual accumulated dose in the groundwork area at operation (A) and shutdown (B) stages.

5. Conclusion

Recently, there have been increasing signals suggesting that anthropogenic ^{3}H releases are expected to rise soon. For instance, some countries are reconsidering the use of nuclear power in response to climate change and the energy crisis, resulting in 57 nuclear reactors are currently under construction worldwide [59]. Additionally, significant progress in nuclear fusion technology, with the first net energy gain of fusion reaction [60], may lead to higher ^{3}H inventory and generation in fusion reactors, potentially posing more tritium contamination issues in the future [61]. Therefore, it is crucial to enhance environmental supervision of tritium contaminations, particularly within nuclear facilities, as an integral part of responsibly utilizing nuclear energy.

This study presents a reliable, efficient, and representative passive monitoring technique based on a new passive sampler design and a tailored HTO analytical protocol. It enables the quantification of airborne tritium contamination in any indoor environment with high spatial and temporal resolution. Unlike conventional 2D profiling of tritium contamination, we presented for the first time, the 3D spatial distribution of HTO in a nuclear reactor hall, revealing significant spatial heterogeneity. Moreover, we provided valuable insights into the application of passive monitoring techniques in estimating tritium release rates and occupational exposure risks.

The developed technique offers a low-cost and convenient tool for regulators to better assess the operational status of nuclear facilities by tracking recorded HTO fluctuations, thereby reducing the risk of nuclear accidents at their sources. It also provides policymakers with valuable information to establish targeted control strategies to address future tritium contamination challenges. Furthermore, the 3D monitoring matrix and its applications hold promise in monitoring and controlling other indoor pollutants.

Although the internal exposure risk of tritium was considered negligible in this thesis, radiation protection concerns regarding HTO should still be addressed in certain environments

with heavy water reactors or compact nuclear facilities, where HTO levels have been reported to be approximately seven orders of magnitude higher than the HTO baseline [62]. Additionally, this work's significance lies in enhancing the visibility of environmental tritium contamination from 2D to 3D, which opens new possibilities for managing radioactivity. By providing more detailed scientific knowledge about radiation levels and risks, eventually fears surrounding radiation will gradually diminish. Thus, the passive monitoring technique is expected to contribute to the development of a practical culture of radiation protection, which is crucial for effective communication with the public and policy implementation in accidental scenarios [63].

6. Bibliography

1) Steinhauser, G., Brandl, A., & Johnson, T. E. Comparison of the Chernobyl and Fukushima nuclear accidents: A Review of the Environmental Impacts. Sci. Total Environ. 2014, 470, 800-450 817. https://doi.org/10.1016/j.scitotenv.2013.10.029

2) Valeska, S. Chernobyl: poverty and stress pose 'bigger threat' than radiation. Nature. 2005 Sep 8; 437(7056):181. https://doi.org/10.1038/437181b

3) Feng, B., Zhuo, W. Levels and behavior of environmental tritium in East Asia. Nucl. Sci Tech 33, 86 (2022). https://doi.org/10.1007/s41365-022-01073-3

4) Qiao, J.; Colgan, W.; Jakobs, G.; Nielsen, S. High-Resolution Tritium Profile in an Ice Core from Camp Century, Greenland. Environ. Sci. Technol.2021, 55, 13638–13645. https://doi.org/10.1021/acs.est.1c01975.

5) Fiévet, B.; Pommier, J.; Voiseux, C.; Bailly Du Bois, P.; Laguionie, P.; Cossonnet, C.; Solier, L. Transfer of Tritium Released into the Marine Environment by French Nuclear Facilities Bordering the English Channel. Environ. Sci. Technol.2013, 47, 6696–6703. https://doi.org/10.1021/es400896t.

6) Eyrolle, F.; Ducros, L.; Le Dizès, S.; Beaugelin-Seiller, K.; Charmasson, S.; Boyer, P.; Cossonnet, C. An Updated Review on Tritium in the Environment. J. Environ. Radioact.2018, 181, 128–137. https://doi.org/10.1016/j.jenvrad.2017.11.001.

7) Nie, B.; Fang, S.; Jiang, M.; Wang, L.; Ni, M.; Zheng, J.; Yang, Z.; Li, F. Anthropogenic Tritium: Inventory, Discharge, Environmental Behavior and Health

Effects. Renew. Sustain. Energy Rev.2021, 135, 110188. https://doi.org/10.1016/j.rser.2020.110188.

8) Lai, J. L.; Li, Z. G.; Wang, Y.; Xi, H. L.; Luo, X. G. Tritium and Carbon-14 Contamination Reshaping the Microbial Community Structure, Metabolic Network, and Element Cycle in the Seawater Environment. Environ. Sci. Technol.2023 Apr 4;57(13):5305-5316. https://doi.org/10.1021/acs.est.3c00422.

9) Kim, S. B.; Baglan, N.; Davis, P. A. Current Understanding of Organically Bound Tritium (OBT) in the Environment. J. Environ. Radioact.2013, 126, 83–91. https://doi.org/10.1016/j.jenvrad.2013.07.011.

10) Feng, B.; Chen, B.; Zhuo, W.; Chen, Q.; Zhang, Y.; Zhang, W. Seasonal and Spatial Distribution of Atmospheric Tritiated Water Vapor in Mainland China. Environ. Sci. Technol.2019, 53, 14175–14185. https://doi.org/10.1021/acs.est.9b03855.

11) Akata, N.; Kakiuchi, H.; Shima, N.; Iyogi, T.; Momoshima, N.; Hisamatsu, S. Tritium Concentrations in the Atmospheric Environment at Rokkasho, Japan before the Final Testing of the Spent Nuclear Fuel Reprocessing Plant. J. Environ. Radioact.2011, 102, 837–842. https://doi.org/10.1016/j.jenvrad.2011.05.005.

12) Kim, S. B.; Stuart, M.; Bredlaw, M.; Festarini, A.; Beaton, D. HT to HTO Conversion and Field Experiments near Darlington Nuclear Power Generating Station (DNPGS) Site. J. Environ. Radioact.2014, 132, 73–80. https://doi.org/10.1016/j.jenvrad.2014.02.001

13) Connan, O.; Bailly du Bois, P.; Solier, L.; Hebert, D.; Voiseux, C. Flux of Tritium from the Sea to the Atmosphere around a Nuclear Reprocessing Plant: Experimental Measurements and Modelling for the Western English Channel. J. Environ. Radioact. 2023, 257, 107068. https://doi.org/10.1016/j.jenvrad.2022.107068.

14) Tanaka, M.; Iwata, C.; Nakada, M.; Kato, A.; Akata, N. Levels of Atmospheric Tritium in the Site of Fusion Test Facility. Radiat. Prot. Dosimetry2022, 198, 1084–1089. https://doi.org/https://doi.org/10.1093/rpd/ncac059.

15) Kotzer, T.; Trivedi, A. Dosimetric Implications of Atmospheric Dispersal of Tritium near a Heavy-Water Research Reactor Facility. Radiat. Prot. Dosimetry2001, 93, 61–66. https://doi.org/https://doi.org/10.1093/oxfordjournals.rpd.a006414.

16) Chen, Z.; Peng, S.; Cheng, S.; Li, Y.; Yang, Y. CFD Calculations of Response Time for Ionization Chambers in Tritium Measurements. Fusion Eng. Des.2019, 143, 196–200. https://doi.org/10.1016/j.fusengdes.2019.03.138.

17) Hou, X. Tritium and 14C in the Environment and Nuclear Facilities: Sources and Analytical Methods. J. Nucl. Fuel Cycle Waste Technol. 2018, 16, 11–39. https://doi.org/10.7733/jnfcwt.2018.16.1.11.

18) Kitamura, K.; Kitabata, T.; Matsushima, A. Development and Experience of Tritium Control in Heavy Water Reactor “Fugen.” Fusion Sci. Technol.2002, 41, 563–567. https://doi.org/10.13182/fst02-a22651.

19) Bae, J. W.; Kang, K. J.; Kim, H. R.; Jeon, S. J. Multi-Channel Plastic-Scintillator-Based Detection System for Monitoring Tritium in Air. Rev. Sci. Instrum.2019, 90. 093304. https://doi.org/10.1063/1.5092543.

20) Feng, B.; Steinhauser, G.; Zhuo, W.; Li, Z.; Yao, Y.; Blenke, T.; Zhao, C.; Renz, F.; Chen, B. Development and Calibration of a Modifiable Passive Sampler for Monitoring Atmospheric Tritiated Water Vapor in Different Environments. Environ. Int.2022, 169, 107505. https://doi.org/10.1016/j.envint.2022.107505.

21) Feng, B.; Chen, B.; Zhao, C.; He, L.; Tang, F.; Zhuo, W. Application of a Liquid Scintillation System with 100-Ml Counting Vials for Environmental Tritium Determination: Procedure Optimization, Performance Test, and Uncertainty Analysis. J. Environ. Radioact.2020, 225, 106427. https://doi.org/10.1016/j.jenvrad.2020.106427.

22) Hirao, S.; Kakiuchi, H. Investigation of Atmospheric Tritiated Water Vapor Level around the Fukushima Daiichi Nuclear Power Plant. Fusion Eng. Des.2021, 171, 112556. https://doi.org/10.1016/j.fusengdes.2021.112556.

23) Feng, B.; Chen, B.; Zhuo, W.; Zhang, W. A New Passive Sampler for Collecting Atmospheric Tritiated Water Vapor. Atmos. Environ.2017, 154, 308–317. https://doi.org/10.1016/j.atmosenv.2017.01.035.

24) Wood, M. J. Outdoor Field Evaluation of Passive Tritiated Water Vapor Samplers at Canadian Power Reactor Sites. Health Phys.1996, 70, 258–267. https://doi.org/10.1097/00004032-199602000-00015.

25) Wood, M. J.; Workman, W. J. G. Environmental Monitoring of Tritium in Air with Passive Diffusion Samplers. Fusion Technol.1992, 21, 529–535. https://doi.org/10.13182/fst92-a29801.

26) Otlet, R. L.; Walker, A. J.; Caldwell-Nichols, C. J. Practical Environmental, Working Area and Stack Discharge Samplers, Passive and Dynamic, for Measurement of Tritium as HTO and HT. Fusion Technol.1992, 21, 550–555. https://doi.org/10.13182/fst92-a29804.

27) Roland A. Jalbert. Monitoring Tritium in Air Containing Other Radioactive Gases. Los Alamos National Lab. 1982, New Mexico, U.S.A.

28) Fukui. M. Development of a Convenient Monitoring Method for Tritiated Water Vapour in Air Using Small Water Dishes as Passive Samplers. Radiat. Prot. Dosimetry1993, 48, 169–178. https://doi.org/doi.org/10.1093/oxfordjournals.rpd.a081861.

29) Vodila, G.; Molnár, M.; Veres, M.; Svingor, É.; Futó, I.; Barnabás, I.; Kapitány, S. Mapping of Tritium Emissions Using Absorption Vapour Samplers. J. Environ. Radioact.2009, 100, 120–124. https://doi.org/10.1016/j.jenvrad.2008.09.012.

30) Miecznik, M.; Mietelski, J. W.; Wójcik-Gargula, A.; Brudecki, K.; Dankowski, J. Search for Tritium in Air in a Room Equipped with 14 MeV Neutron Generator with Tritiated Targets. J. Environ. Radioact.2020, 217. https://doi.org/10.1016/j.jenvrad.2020.106218.

31) Kim, D.; Croudace, I. W.; Warwick, P. E. The Requirement for Proper Storage of Nuclear and Related Decommissioning Samples to Safeguard Accuracy of Tritium Data. J. Hazard. Mater. 2012, 213–214, 292–298. https://doi.org/10.1016/j.jhazmat.2012.01.094.

32) Dae, J. K.; Warwick, P. E.; Croudace, I. W. Tritium Speciation in Nuclear Reactor Bioshield Concrete and Its Impact on Accurate Analysis. Anal. Chem.2008, 80, 5476–5480. https://doi.org/10.1021/ac8002787.

33) Tipler, P.A., Mosca, G., 2015. Physik für Wissenschaftler und Ingenieure: [der Begleiter bis zum Bachelor], 7. dt. Aufl., Lehrbuch. Springer Spektrum, Berlin; Heidelberg. https://doi.org/10.1007/978-3-642-54166-7

34) Demtröder, W., 2014. Experimentalphysik 4: Kern-, Teilchen- und Astrophysik, 4. Aufl. 2014. ed, SpringerLink : Bücher. Springer Spektrum, Berlin, Heidelberg. https://doi.org/10.1007/978-3-642-21476-9

35) Villa, M, 2020. Skriptum Reaktorphysik, TU Wien, Austria

36) National Diagnostics Laboratory Staff, 2004. Principles and Applications of Liquid Scintillation Counting - A PRIMER FOR ORIENTATION. National Diagnostics.

37) US EPA, O., 2015. Radionuclide Basics: Tritium [WWW Document]. URL:https://www.epa.gov/radiation/radionuclide-basics-tritium (accessed 6. May.23).

38) Tritium and ^{14}C in the Environment and Nuclear Facilities: Sources and Analytical Methods, 2018. Journal of Nuclear Fuel Cycle and Waste Technology 16, 11–39.

39) Cauquoin, A., Jean-Baptiste, P., Risi, C., Fourré, É., Landais, A., 2016. Modeling the global bomb tritium transient signal with the AGCM LMDZ-iso: A method to evaluate aspects of the hydrological cycle. Journal of Geophysical Research: Atmospheres 121, 612-629. https://doi.org/10.1002/2016JD025484

40) Laboratory Training Manual on the Use of Nuclear and Associated Techniques in Pesticide Residues, 1991. Technical Reports Series. INTERNATIONAL ATOMIC ENERGY AGENCY, Vienna.

41) Management of Tritium at Nuclear Facilities, 1984. Technical Reports Series. INTERNATIONAL ATOMIC ENERGY AGENCY, Vienna.

42) L'Annunziata, M.F., Tarancón, A., Bagán, H., García, J.F., 2020. Chapter 6 - Liquid scintillation analysis: principles and practice, in: L'Annunziata, M.F. (Ed.), Handbook of Radioactivity Analysis (Fourth Edition). Academic Press, pp. 575–801. https://doi.org/10.1016/B978-0-12-814397-1.00006-6

43) Hou, X. Radiochemical Analysis of Radionuclides Difficult to Measure for Waste Characterization in Decommissioning of Nuclear Facilities. J. Radioanal. Nucl. Chem. 2007, 273, 43–48. https://doi.org/10.1007/s10967-007-0708-x.

44) Munyon, W. J.; Reilly, D. W.; Webb, J. AGHCF Gaseous-Effluent Tritium Sampling System: Design Considerations and Performance Testing Results. Health Phys. 2008, 94, 75–85. https://doi.org/10.1097/01.HP.0000279630.18757.80.

45) Waidhofer, D. 2023. Projektarbeit, TRIGA Center Atominstitut, TU Wien

46) Blondel, A.; Plaisance, H. Screening of Formaldehyde Indoor Sources and Quantification of Their Emission Using a Passive Sampler. Build. Environ. 2011, 46, 1284–1291. https://doi.org/10.1016/j.buildenv.2010.12.011.

47) Shah, M. M. Improved Method for Calculating Evaporation from Indoor Water Pools. Energy Build. 2012, 49, 306–309. https://doi.org/10.1016/j.enbuild.2012.02.026.

48) Murray, F. W. On the Computation of Saturation Vapor Pressure. J. Appl. Meteorol. 1967, 6, 203–204.

49) Marang, L.; Siclet, F.; Luck, M.; Maro, D.; Tenailleau, L.; Jean-Baptiste, P.; Fourré, E.; Fontugne, M. Modelling Tritium Flux from Water to Atmosphere: Application to the Loire River. J. Environ. Radioact. 2011, 102, 244–251. https://doi.org/10.1016/j.jenvrad.2010.11.015.

50) Nie, B.; Yang, J.; Yuan, Y.; Li, F. Additional Radiation Dose Due to Atmospheric Dispersion of Tritium Evaporated from a Hypothetical Reservoir. Appl. Radiat. Isot. 2021, 167, 109475. https://doi.org/10.1016/j.apradiso.2020.109475.

51) Zhang, X.; Wong, C.; Lei, Y. D.; Wania, F. Influence of Sampler Configuration on the Uptake Kinetics of a Passive Air Sampler. Environ. Sci. Technol. 2012, 46, 397–403. https://doi.org/10.1021/es203292x.

52) Das, H. A.; Hou, X. Steady-State Leaching of Tritiated Water from Silica Gel. J. Radioanal. Nucl. Chem. 2009, 280, 467–468. https://doi.org/10.1007/s10967-009-7458-x.

53) Campling, D.; Macheta, P.; Patel, B.; Schofield, P. Tritium-in-Air "bubbler" Samplers and Internal Radiation Doses at Jet. Fusion Sci. Technol. 2002, 41, 525–527. https://doi.org/10.13182/fst02-a22644.

54) Kim, C. K.; Rho, B. H.; Lee, K. J. Environmental Tritium in the Areas Adjacent to Wolsong Nuclear Power Plant. J. Environ. Radioact. 1998, 41, 217–231. https://doi.org/10.1016/S0265-931X(97)00093-3.

55) Connan, O.; Hébert, D.; Solier, L.; Maro, D.; Pellerin, G.; Voiseux, C.; Lamotte, M.; Laguionie, P. Atmospheric Tritium Concentrations under Influence of AREVA NC La Hague Reprocessing Plant (France) and Background Levels. J. Environ. Radioact. 2017, 177, 184–193. https://doi.org/10.1016/j.jenvrad.2017.06.015.

56) Fukui, M. Locating Tritium Sources in a Research Reactor Building. Health Phys. 2005, 89, 303–314. https://doi.org/10.1097/01.HP.0000161281.51407.a4.

57) Fukui, M.; Kimura, S. Oxidized Tritium around a Research Reactor Site. J. Nucl. Sci. Technol. 2005, 42, 816–824. https://doi.org/10.1080/18811248.2004.9726451.

58) Steinhauser, G.; Villa, M. Dihydrogen Gas Emission of a 250kWth Research Reactor. Appl. Radiat. Isot. 2011, 69, 1618–1620. https://doi.org/10.1016/j.apradiso.2011.05.010.

59) IAEA. The Database on Nuclear Power Reactors. Power Reactor Information System (PRIS). https://pris.iaea.org/PRIS/home.aspx.

60) Weir, B. This Lab Achieved a Stunning Breakthrough on Fusion Energy. CNN. May 12, 2023. https://edition.cnn.com/2023/05/12/us/fusion-energy-livermore-lab-climate/index.html.

61) Chen, D.; Nie, B.; Dong, B.; Yang, D.; Wu, S.; He, J.; Gu, W.; Wang, D. Insights into Near-Surface Distribution Characteristics of Multi-Form Tritium with Consideration of Atmospheric Buoyancy and Gravitational Deposition. Chemosphere 2023, 312, 137231. https://doi.org/10.1016/j.chemosphere.2022.137231.

62) Hou, X. Analysis of Urine for Pure Beta Emitters: Methods and Application. Health Phys. 2011, 101, 159–169. https://doi.org/10.1097/HP.0b013e31821497c0.

63) Lochard, J.; Chhem, R. K. Lessons from Fukushima: The Power of Culture as Storytelling. Lancet 2023, 401, 1650–1651. https://doi.org/10.1016/S0140-6736(23)00719-5.

7. Appendix

Table A1. Detailed information on airborne HTO in the reactor hall.

No.	Uptake (g)	^{3}H specific activity ± uncertainty (Bq L^{-1})	HTO volumetric concentration ± uncertainty (mBq m^{-3})	Note
1	1.88	23.84 ± 23.84	85.12 ± 85.12	<MDA
2	3.26	14.23 ± 14.23	103.26 ± 103.26	<MDA
3	1.28	34.42 ± 34.42	79.05 ± 79.05	<MDA
4	1.41	31.34 ± 31.34	80.24 ± 80.24	<MDA
5	0.79	55.04 ± 55.04	74.74 ± 74.74	<MDA
6	1.63	27.34 ± 27.34	82.59 ± 82.59	<MDA
7	1.72	25.98 ± 25.98	83.54 ± 83.54	<MDA
8	1.64	27.23 ± 27.23	82.85 ± 82.85	<MDA
9	1.58	28.22 ± 28.22	82.26 ± 82.26	<MDA
10	1.88	23.85 ± 23.85	85.17 ± 85.17	<MDA
11	1.66	26.89 ± 26.89	82.96 ± 82.96	<MDA
12	1.76	25.48 ± 25.48	84.18 ± 84.18	<MDA
13	2.04	22.05 ± 22.05	86.87 ± 86.87	<MDA
14	2.09	21.56 ± 21.56	87.43 ± 87.43	<MDA
15	0.91	48.03 ± 48.03	75.90 ± 75.90	<MDA
16	1.25	35.37 ± 35.37	79.10 ± 79.10	<MDA
17	1.45	30.55 ± 30.55	80.71 ± 80.71	<MDA
18	2.1	21.45 ± 21.45	87.52 ± 87.52	<MDA
19	1.95	22.98 ± 22.98	85.72 ± 85.72	<MDA
20	1.89	57.72 ± 15.40	207.42 ± 55.33	
21	1.26	35.11 ± 35.11	79.23 ± 79.23	<MDA
22	1.27	34.74 ± 34.74	79.09 ± 79.09	<MDA
23	1.15	38.19 ± 38.19	77.87 ± 77.87	<MDA
24	1.85	24.27 ± 24.27	85.03 ± 85.03	<MDA
25	2.79	16.49 ± 16.49	96.55 ± 96.55	<MDA
26	1.12	39.29 ± 39.29	77.82 ± 77.82	<MDA
27	1.2	36.68 ± 36.68	78.39 ± 78.39	<MDA
28	1.3	33.96 ± 33.96	79.34 ± 79.34	<MDA
29	1.98	22.70 ± 22.70	86.26 ± 86.26	<MDA
30	1.34	33.08 ± 33.08	79.96 ± 79.96	<MDA
31	1.38	32.04 ± 32.04	80.06 ± 80.06	<MDA
32	1.31	33.82 ± 33.82	79.70 ± 79.70	<MDA
33	1.91	23.53 ± 23.53	85.63 ± 85.63	<MDA
34	1.18	37.33 ± 37.33	78.32 ± 78.32	<MDA
35	0.77	56.66 ± 56.66	74.86 ± 74.86	<MDA
36	1.29	34.19 ± 34.19	79.21 ± 79.21	<MDA
37	1.41	31.38 ± 31.38	80.33 ± 80.33	<MDA
38	1.26	35.09 ± 35.09	79.17 ± 79.17	<MDA
39	1.26	35.10 ± 35.10	79.21 ± 79.21	<MDA
40	0.74	58.94 ± 58.94	74.65 ± 74.65	<MDA
41	1.14	38.53 ± 38.53	77.83 ± 77.83	<MDA

Continued Table A1

No.	Uptake (g)	^{3}H specific activity ± uncertainty (Bq L^{-1})	HTO volumetric concentration ± uncertainty (mBq m^{-3})	Note
42	1.29	34.21 ± 34.21	79.25 ± 79.25	<MDA
43	2.12	85.83 ± 13.69	354.19 ± 56.51	
44	1.49	104.70 ± 19.60	285.33 ± 53.42	
45	1.76	82.89 ± 16.67	273.83 ± 55.08	
46	1.16	38.00 ± 38.00	78.22 ± 78.22	<MDA
47	1.07	41.03 ± 41.03	77.30 ± 77.30	<MDA
48	1.67	26.74 ± 26.74	83.09 ± 83.09	<MDA
49	1.35	32.75 ± 32.75	79.82 ± 79.82	<MDA
50	1.71	115.71 ± 17.56	369.57 ± 56.08	
51	1.14	38.51 ± 38.51	77.78 ± 77.78	<MDA
52	1.22	36.08 ± 36.08	78.54 ± 78.54	<MDA
53	2.09	21.64 ± 21.64	87.76 ± 87.76	<MDA
54	1.72	25.97 ± 25.97	83.52 ± 83.52	<MDA
55	0.75	58.04 ± 58.04	74.57 ± 74.57	<MDA
56	1.12	39.19 ± 39.19	77.62 ± 77.62	<MDA
57	1.23	35.85 ± 35.85	78.76 ± 78.76	<MDA
58	1.27	34.77 ± 34.77	79.15 ± 79.15	<MDA
59	1.46	30.34 ± 30.34	80.81 ± 80.81	<MDA
60	0.77	241.28 ± 38.11	318.79 ± 50.35	
61	1.24	35.55 ± 35.55	78.81 ± 78.81	<MDA
62	0.85	209.93 ± 33.91	308.26 ± 49.79	
63	1.22	36.08 ± 36.08	78.54 ± 78.54	<MDA
64	1.03	42.51 ± 42.51	76.82 ± 76.82	<MDA
65	1.2	109.41 ± 24.15	233.84 ± 51.63	
66	1.09	40.35 ± 40.35	77.57 ± 77.57	<MDA
67	1.1	83.88 ± 26.28	162.88 ± 51.04	
68	1.12	39.22 ± 39.22	77.69 ± 77.69	<MDA
69	2.25	72.62 ± 13.29	322.47 ± 59.05	
70	2.32	50.89 ± 13.02	234.76 ± 60.07	
71	1.2	36.71 ± 36.71	78.46 ± 78.46	<MDA
72	1.17	37.56 ± 37.56	78.06 ± 78.06	<MDA
73	1.32	33.50 ± 33.50	79.62 ± 79.62	<MDA
74	1.02	195.55 ± 28.73	349.65 ± 51.38	
75	1.56	28.57 ± 28.57	82.06 ± 82.06	<MDA
76	1.68	68.65 ± 17.42	214.81 ± 54.51	
77	2.1	21.54 ± 21.54	87.88 ± 87.88	<MDA
78	1.63	27.46 ± 27.46	82.97 ± 82.97	<MDA
79	1.63	67.74 ± 18.30	204.65 ± 55.29	
80	0.98	44.81 ± 44.81	76.72 ± 76.72	<MDA
81	1.39	199.43 ± 21.68	502.31 ± 54.60	
82	1.54	161.54 ± 18.83	457.13 ± 53.29	
83	1.59	165.30 ± 18.73	485.26 ± 55.00	
84	1.59	160.97 ± 18.79	472.55 ± 55.16	
85	0.98	448.78 ± 31.04	768.28 ± 53.15	

Continued Table A1

No.	Uptake (g)	^{3}H specific activity ± uncertainty (Bq L^{-1})	HTO volumetric concentration ± uncertainty (mBq m^{-3})	Note
86	1.39	375.26 ± 21.69	945.19 ± 54.65	
87	1.46	234.28 ± 20.54	623.84 ± 54.71	
88	1.05	165.74 ± 27.74	305.87 ± 51.21	
89	1.22	203.92 ± 24.20	443.89 ± 52.68	
90	1.07	239.99 ± 28.25	452.12 ± 53.23	
91	1.2	223.84 ± 25.06	478.41 ± 53.57	
92	1.14	205.58 ± 25.78	415.18 ± 52.06	
93	0.95	184.32 ± 30.52	305.09 ± 50.52	
94	1.03	456.48 ± 29.15	824.91 ± 52.68	
95	1.07	384.11 ± 27.91	723.62 ± 52.59	
R1	0.77	459.1±37.59	626.46 ± 49.67	
R2	0.72	599.1±40.72	761.20 ± 50.09	
R3	0.65	410.4±44.19	468.04 ± 48.80	